NASA TN D-752

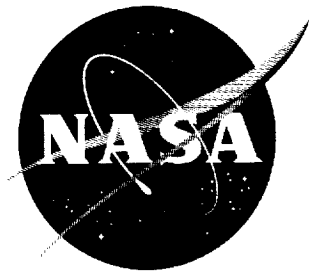

TECHNICAL NOTE

D-752

AERODYNAMIC CHARACTERISTICS OF PARACHUTES AT MACH NUMBERS FROM 1.6 TO 3

By Julian D. Maynard

Langley Research Center
Langley Field, Va.

NATIONAL AERONAUTICS AND SPACE ADMINISTRATION
WASHINGTON

May 1961

NATIONAL AERONAUTICS AND SPACE ADMINISTRATION

TECHNICAL NOTE D-752

AERODYNAMIC CHARACTERISTICS OF PARACHUTES AT MACH NUMBERS FROM 1.6 TO 3

By Julian D. Maynard

SUMMARY

A wind-tunnel investigation has been conducted to determine the parameters affecting the aerodynamic performance of drogue parachutes in the Mach number range from 1.6 to 3. Flow studies of both rigid- and flexible-parachute models were made by means of high-speed schlieren motion pictures and drag coefficients of the flexible-parachute models were measured at simulated altitudes from about 50,000 to 120,000 feet.

Porosity and Mach number were found to be the most important factors influencing the drag and stability of flexible porous parachutes. Such parachutes have a limited range of stable operation at supersonic speeds, except for those with very high porosities, but the drag coefficient decreases rapidly with increasing porosity.

INTRODUCTION

The safe recovery of man-carrying vehicles, instrumented capsules, and large expensive first-stage rocket boosters demands the use of reliable and efficient decelerators. An analysis in reference 1 indicates that lightweight drogue parachutes, which may be deployed at will for deceleration and stabilization, may provide more drag for a given amount of bulk and weight than other types of decelerators. Current advances in the development of high-strength fabric materials capable of withstanding high temperatures indicate the practicability of such decelerators at supersonic speeds.

It was pointed out in reference 2 that stability and drag coefficient are the two criteria to be used in evaluating the aerodynamic performance of decelerators. Usually, the bodies to be recovered (the payloads) are high-drag shapes which by themselves achieve high deceleration rates. Thus, the problem is to produce a concentrated drag at some particular point on the body to keep it from tumbling and to maintain some predetermined attitude during the free fall. Stability of the applied drag force, as well as the dynamic stability of the payload-and-drogue combination, are most important. Drag coefficient, on the other

hand, may be considered to be a measure of decelerator efficiency, particularly if fabric or construction area is used which reflects the weight of the decelerator.

Some early tests of fabric ribbon parachutes indicated that these parachutes produced only 20 percent of the anticipated drag at supersonic speeds and were subject to violent instability. The purpose of this paper is to present the results of an investigation made in the Langley Unitary Plan wind tunnel to study the flow field about small parachute canopies at supersonic speeds and to determine the parameters affecting the aerodynamic performance of drogue parachutes in the Mach number range from 1.6 to 3. Flow studies of both rigid- and flexible-parachute models were made by means of high-speed schlieren motion pictures, and drag coefficients of the flexible models were measured at simulated altitudes from about 50,000 to 120,000 feet. Some effects of canopy porosity, reefing, and payload wake are included.

The weight factor, construction details, and deployment problems will no doubt require careful design studies of full-scale models. Dynamic stability problems of the payload-and-drogue combination must be solved by a consideration of the inertia forces and development of proper towline attachments. Some results of such studies may be found in references 3 and 4.

SYMBOLS

b	distance between horizontal parachute ribbons, in.
B_{hr}	horizontal parachute ribbon width, in.
C_D	drag coefficient, $\frac{\text{Drag}}{q(S_o \text{ or } S_p)}$
c_o	constructed porosity, S_v/S_o
D_o	nominal (laid-out-flat) diameter of the parachute canopy, ft
D_p	projected, or frontal, diameter of the inflated parachute canopy, assumed to be $2/3D_o$
M	Mach number
M_{cr}	critical Mach number

q dynamic pressure, lb/sq ft

S_o total cloth area of parachute canopy including slots and vent, $\frac{\pi D_o^2}{4}$, sq ft

S_p projected, or frontal, area of the inflated parachute canopy, $\frac{\pi D_p^2}{4}$, sq ft

S_v vented area of ribbon parachute canopy (including center vent), sq ft

t time, sec

APPARATUS AND MODELS

Wind Tunnel

The tests were conducted in the Langley Unitary Plan wind tunnel. The tunnel has two test sections of the variable-pressure return-flow type. The test sections are 4 feet square and approximately 7 feet in length. The nozzles leading to the test sections are of the asymmetric sliding-block type, and the Mach number may be varied continuously through a range from 1.5 to 2.8 in one test section and from 2.3 to 4.65 in the other. Further details of the wind tunnel may be found in reference 5.

Rigid-Parachute Models

The rigid-parachute models were designed to simulate a parachute with an inflated ribbon canopy. The canopy was made by spinning a stainless-steel sheet in which a pattern of rectangular slots was cut to form the ribbons. The vertical ribbons, normally found on ribbon parachutes, were omitted to facilitate fabrication. The contour of the canopy was that which would be formed by the gore center lines of a flat, circular parachute canopy. Details of this canopy shape are shown in figure 1. The gore layouts for the various 24-gore rigid canopies (I to VI) tested are shown in figure 2. Canopy I had slots which provided a porosity of 20 percent. These slots were modified by cutting out some of the solid material between slots to form canopy II, which had a porosity of 24 percent. Both canopies I and II had no center vent and were supported by a single sting from the wind-tunnel support system as shown in figure 3(a). Canopies III, IV, V, and VI, with porosities of

35, 45, 36.5, and 28 percent, respectively, had center vents varying from 1.14 to 5.714 inches in diameter as shown in figure 2. For this reason the sting support was modified as shown in figure 3(b) to support the canopies having a center vent. Since the rigid canopies were used for flow studies only, they were not mounted on a balance and, therefore, no drag measurements were made.

Shroud lines for the rigid canopies were made from 1/8-inch-diameter steel rods in lengths of 1 and 2 feet in order to determine the effect of shroud-line length on the aerodynamic characteristics of the model. Each shroud line was removable so that the effect of the number of shroud lines could be investigated.

The various configurations of the rigid canopies are listed in table I. In one configuration having six 12-inch shroud lines "flow stabilizers" in the form of small disks were attached to each shroud line 4 inches upstream of the canopy skirt, as shown in figure 3(b).

Flexible-Parachute Models

Most of the flexible-parachute models tested are listed in table II and photographs of some of the parachutes, including the more unconventional ones, are shown in figure 4. Gore details of most of the parachutes are shown in figure 5. The nominal diameter of the models ranged from 1.25 to 0.5 feet, and the porosity ranged from 1 to 83 percent. Parachute 1a was made by sewing cloth over each gore of parachute 1, leaving only the center vent as shown in figure 4(b). Parachute 2 was slightly less porous than parachute 1 and had a different gore pattern. Parachute 3 was similar to parachute 2 but was considerably larger. Parachute 4 was not made up of gores but of a net to provide a porosity of 50 percent. The canopy skirt was gathered to form a circle having a diameter two-thirds of the nominal diameter and eight equally spaced shroud lines were attached so that, in effect, there were eight gores. (See fig. 4(e).) Parachute 5 (fig. 4(f)) was made by removing the horizontal ribbons from parachute 8 and sewing a highly porous nylon net over the entire canopy. Parachute 6 (fig. 4(g)) was also made by sewing a net over the gores of a ribbon parachute after removing the horizontal ribbons. Parachute 7, the most porous of any tested, was made of net in a manner similar to parachute 4. (See fig. 4(h).)

Parachutes 8, 9, and 10 were similar except for the size of the center vent, which provided a porosity variation from 20 to 40.5 percent. A photograph of parachute 9 is shown in figure 4(i). Parachute 11 was a small parachute rigged for testing in a three-chute cluster. Parachute 12 had, in addition to the usual shroud lines, a line attached to the center vent which pulled the vent in to a point just downstream of

the canopy skirt. Parachutes 13, 14, and 15 were designed to provide a variation in the ratio of the space between horizontal ribbons to the ribbon width b/B_{hr}. This ratio was 1.5, 0.586, and 1.145 for parachutes 13, 14, and 15, respectively. Parachute 15a was made by attaching a rubber ring to the canopy skirt of parachute 15 as shown in figure 4(j). The outside diameter of the rubber ring was 7 inches, and the diameter of a cross section through the ring was 5/8 inch. The rubber ring was added to simulate an inflatable ring which might be used to stiffen the canopy skirt and thus aid in holding the parachute open. Parachutes 16 and 17 had canopies with 45° and 30° conical shapes, respectively. Parachute 17a was made by modifying parachute 17 so that the canopy would be held rigidly open with small steel rods as shown in figure 4(k). Also, very short shroud lines were attached to a small rigid ring within the canopy as shown in the photograph of figure 4(k).

Reefed parachute.- Another parachute, not listed in table II, was tested with various amounts of reefing. This parachute was a conventional ribbon type with a nominal diameter of 1.73 feet and a porosity of 28 percent.

Rotochute.- In addition to the flexible-parachute models just described, a rotochute with a cloth area of 0.314 square foot was included as one of the test models. A photograph of this rotochute, or "vortex ring" parachute, is shown in figure 4(l).

Support System and Deployment Mechanism for Flexible-Parachute Models

Figure 6 is a sketch of the flexible-parachute test installation in the wind tunnel and figure 7 shows photographs of the installation. Two support struts are mounted from the wind-tunnel side walls in a horizontal plane on the tunnel center line. The struts taper in both planform and thickness from a chord of 12 inches and thickness of 1/2 inch at the tunnel wall to a chord of 6 inches and thickness of 1/4 inch at the tunnel center line. The leading and trailing edges of the struts are sharpened, and the leading edge is swept back 55°. A conical-nosed cylindrical body 2.25 inches in diameter and about 21 inches long was supported by the struts on the tunnel center line. The parachute deployment mechanism was contained in the cylindrical body, in which a piston was actuated by a 1-grain powder squib to push the parachute out the downstream end of the cylinder. After packing the parachute and riser line in the cylinder, small nylon threads were tied across the end of the cylinder to hold the parachute in place until the piston was actuated by firing the squib. Upon firing the squib, which was done remotely, the piston pushed against the parachute pack with sufficient force to break the threads and allow the parachute to be deployed into the airstream.

A 1/8-inch-diameter woven nylon cord about 24 inches long was used as a riser line for most of the tests. The riser line was attached to a small ball-bearing swivel which, in turn, was attached to a simple strain-gage balance to measure the drag force. The swivel was necessary to prevent twisting of the riser and shroud lines, since the parachutes had a tendency to rotate at times. The strain-gage balance was rigidly mounted to the support system within the cylinder.

In order to obtain some evaluation of the effects of the wake from the payload on parachute operation, the cylindrical body was replaced for some of the tests by a 1/10-scale model of the Project Mercury manned capsule. Figure 8 is a sketch of this capsule mounted in the wind tunnel for tests of the drogue parachutes and figure 9 shows photographs of the capsule in the test section. Although it would be desirable to have no central body upstream of the capsule model in order to simulate properly the wake behind the capsule, this was not feasible since it was necessary to use the existing strut support system. The 1/10-scale capsule model was, therefore, mounted as shown in figure 8.

For tests of the reefed parachute the straight cylindrical body was replaced by the conical body sketched in figure 10. Also, the strain-gage balance used to measure drag was replaced by a spring scale located outside the test section and attached to the reefed parachute by means of a cable which ran through one of the support struts and the conical body.

TESTS

Rigid-Parachute Models

The test conditions for each configuration of the rigid-parachute models are shown in table I. The Reynolds numbers for these tests ranged from about 700,000 to 1,000,000 per foot. Although no drag data were obtained in these tests, high-speed schlieren motion pictures were taken for each test condition. The camera speed varied from about 500 to 3,500 frames per second, but most of the film was made at a camera speed of about 2,000 frames per second. As indicated in table I, most of the rigid-parachute models were tested at 0° angle of attack, but a few tests were at other angles of attack up to 5°.

Flexible-Parachute Models

The test conditions for the flexible-parachute models are given in table II. Since flexible parachutes 1 and 2 were the most stable of any

tested, they were also investigated over the range of Mach numbers shown in table III.

All the flexible-parachute models were towed behind bodies mounted on struts upstream of the models, and for this reason preliminary tests were made to determine what riser line length and Mach number could be used in the wind-tunnel tests to avoid interference from wall-reflected shock waves. The riser-line length chosen (24 inches) was about 10.7 times the base diameter (2.25 inches) of the forebody, or payload.

In some of the tests the flexible parachutes were deployed after establishing the test conditions in the wind tunnel and in other tests a small string was used to apply tension to the parachute and tow cable so that the parachute was suspended in the test section before starting airflow through the tunnel. In these tests the small string was broken after supersonic flow was established, so that the parachute was freely suspended on the tow cable only. In tests where the parachute was deployed after establishing the test conditions, a timing device was used to start the high-speed camera 1 second before the squib was fired to deploy the parachute. This sequence insured obtaining pictures of the deployment and allowed time for the camera to get up to speed. Several measurements of the drag force were made at each Mach number and the results were averaged. No satisfactory dynamic records of the drag force were obtained.

The test condition for each configuration of the reefed parachute is given in table IV. This parachute was towed behind the conical body sketched in figure 10 and the riser-line length was 24 inches, or only about 4.9 times the base diameter (4.9 inches) of the payload.

In all tests of the rotochute at supersonic speeds a failure occurred before drag data could be obtained. However, in one test the failure did not occur until about 1 minute after deployment, and a high-speed schlieren motion picture was obtained during this interval. In this test the parachute was deployed behind the conical-nosed cylindrical body (2.25 inches in diameter). The riser line was 24 inches long and was attached to the cylindrical body through a heavy-duty swivel and to the rotochute through a smaller swivel. The Mach number during this test was approximately 2.2 and the dynamic pressure was 150 pounds per square foot.

Accuracy

Based on the strain-gage-balance calibration and repeatability of the data, the values of average drag coefficient when the parachutes were fairly stable are believed to be accurate to within ± 0.02. In the reefed-parachute tests, where a simple spring balance was used, the drag coefficients are believed to be accurate to within ± 0.04. A calibration was

made of the spring balance and the tare force caused by friction between the long cable and its conduit was evaluated. Values of Mach number are accurate to ±0.015.

RESULTS AND DISCUSSION

The results of the investigation of the parameters affecting the aerodynamic performance of drogue parachutes are given in tables I to IV and in figures 11 to 22. A motion-picture film supplement has also been prepared and is available on loan. A request card form and a description of the film will be found at the back of this paper, on the page immediately preceding the abstract and index pages.

Rigid-Parachute Models

A study of the high-speed schlieren motion pictures made in tests of the rigid-parachute models results in several significant observations concerning the flow about parachute canopies at supersonic speeds. In tests of canopies I and II without shroud lines the bow shock changed intermittently from a symmetrical to an unsymmetrical pattern as shown in figure 11, which is a series of enlargements of the frames from the motion-picture film. At times the bulging shock pattern appeared to rotate about the canopy. This odd phenomenon has been observed in heat-transfer studies of reentry bodies with cup-faced noses. When a center vent was added and the porosity increased to 28, 35, or 45 percent (canopies VI, III, and IV, respectively) the bow shock was symmetrical as shown in figure 12. The unsymmetrical shock patterns on the lower-porosity canopies would no doubt result in unsymmetrical forces which would cause violent oscillations (in a plane perpendicular to the free airstream) of a parachute towed on a flexible cable.

The addition of 24 shroud lines to a canopy changed the flow pattern considerably as shown in figure 13. The very rapid distortion of the bow wave was apparently caused by the tendency of the normal or secondary shock to detach from the skirt of the canopy and move upstream, thus distorting the bow wave. This unsteady-flow phenomenon occurred on all the rigid canopies (porosities 20 to 45 percent) with shroud lines, but was more pronounced with the shorter shroud lines than for the longer ones as shown in the film supplement. Changing the number of shroud lines had little effect on the shock pattern, as shown in figure 14, and failed to eliminate the unsteady-flow phenomenon. The addition of the flow stabilizers on the shroud lines also failed to eliminate the unsteady flow as shown in figure 15.

The results of the rigid-parachute tests indicate that conventional ribbon parachutes (with porosities from 20 to 45 percent) in a normally inflated condition will experience unsteady-flow conditions at supersonic speeds which may adversely affect their operation. Variations in porosity and in the length and number of shroud lines failed to eliminate the unsteady-flow phenomenon, but increasing the canopy porosity and adding a center vent may eliminate an unsymmetrical shock pattern which might cause violent oscillations in a plane perpendicular to the free airstream. Further discussion of these rigid-parachute tests may be found in reference 6.

Flexible-Parachute Models

Stability.- It has been said that parachute design is an art rather than a science and there is very little published data to indicate otherwise. This is particularly true about parachutes for use at supersonic speeds. The wide variety of flexible-parachute-model characteristics listed in table II is some indication of the need for a systematic study of various parameters affecting parachute operation at supersonic speeds. The parachutes listed in table II were obviously not made for a systematic investigation but a careful analysis of the high-speed schlieren motion pictures made during tests of these parachutes leads to several significant observations concerning porous-parachute stability.

First, there apparently exists an important relation between porosity, Mach number, and stability of flow. For example, parachute 1a, which had a porosity of only 1 percent, was so unstable at a Mach number of 3.1 that violent oscillations from side to side and up and down caused a failure which prevented taking motion pictures. Parachute 3, with a porosity of 19 percent, also suffered the same failure at a Mach number of 3.1. However, parachute 1, which was quite similar to parachute 3, was relatively stable at a Mach number of 2.0. Also, parachute 2, with a porosity of 19 percent, was relatively stable at a Mach number of 2.0, although it was towed behind a different payload which probably caused a different wake in which the parachute must operate. Parachutes 1 and 2 were equally stable when towed behind the same payload at a Mach number of 2.0, although there was a difference in their drag coefficients. (See table III.)

These results indicate that a flexible porous parachute with a constructed porosity of approximately 20 percent is stable at a Mach number of 2, but violently unstable at a Mach number of 3. It is also violently unstable at a Mach number of 3 if the constructed porosity is reduced to 1 percent by closing all but the center vent (parachute 1a). If the Mach number is held constant at approximately 2 and the constructed porosity is increased to 40.5 percent (parachute 8), the parachute becomes very

unstable, but the instability is of a different type. Instead of violent oscillations from side to side and up and down, the parachute alternately inflates and collapses in a "breathing" motion. Further increase in porosity to 83 percent (parachute 7) eliminates this breathing instability at a Mach number of 2.

Apparently there are different regions of stable and unstable parachute operation depending upon Mach number and porosity. Furthermore, the unstable regions are characterized by different types of instability. It may be recalled that one type of unstable flow was indicated for low-porosity parachutes in the rigid-canopy tests and another type for the higher porosity models with shroud lines. However, the rigid parachute models with a porosity of 20 percent had an unstable type of flow, and the flexible parachutes of the same constructed porosity were relatively stable at a Mach number of 2. It appears, therefore, that the flexible parachutes have an effective porosity which differs from the constructed porosity, and it appears that the flexible parachutes will present stability characteristics different from those for rigid parachutes of the same constructed porosity. L 7 2 3

In the tests of the flexible-parachute models no motion pictures were obtained showing the violent oscillations (from side to side and up and down) of the low-porosity parachutes because of the rapid failure of the models. However, these violent oscillations were observed by eye before failure. The other type of unstable flow, characterized by breathing of the parachute canopy, may easily be seen in the high-speed schlieren motion pictures of some of the flexible parachutes. Figure 16 illustrates this type of unstable flow, and because the canopy is inflated, then partially collapsed, and reinflated, this type of flow is referred to as inflation instability.

A careful study of the high-speed schlieren motion pictures made during these tests leads to a hypothesis concerning inflation instability of flexible ribbon parachutes. Since such parachutes are porous, they have a critical Mach number at which choking takes place. This critical Mach number is determined by the ratio of the frontal or capture area to the open area of the porous parachute. The photographs in figure 16 indicate that the canopy is inflated when choked and partially collapsed when the shock is swallowed. Obviously, when something happens which reduces the capture area, the area ratio is reduced and therefore the critical Mach number may be lowered to a point where the shock will be swallowed. However, since the canopy partially collapses when the shock is swallowed, the vented area of the canopy is sharply reduced thereby increasing the area ratio and the critical Mach number so that the shock is expelled and the canopy is again inflated because of the choked condition. This phenomenon is of a cyclic nature with a very high frequency (100 to 200 cycles per second) and is somewhat analogous to the inlet buzz phenomenon. The

action which starts the fluctuations by reducing the capture area is the familiar interaction between the boundary layer on the individual shroud lines and the shock wave caused by the parachute canopy. This interaction, which is unsteady, causes a "dead air" region around the shroud lines upstream of the canopy which partially blocks the entrance and thereby reduces the capture area.

This simplified explanation of the inflation instability encountered in porous-parachute operation at supersonic speeds will assist in the prediction of the stability regions of such parachutes. Figure 17 has been prepared from the results of the present tests to show estimated stability regions as a function of porosity and Mach number. Porosity is plotted against Mach number from 1.5 to 3.0. In the lower porosity region the bow shock is unsymmetrical, resulting in violent oscillations (from side to side and up and down) and a very unstable parachute. Increasing the porosity at Mach numbers below 2.5 may place the parachute in the limited stable region where the bow shock remains in front of the canopy and has a symmetrical pattern as illustrated in the figure. For parachutes of very high porosity (80 percent), the canopy is partially collapsed and a normal shock forms downstream of the canopy as shown. Such a configuration may be stable but will have a low drag coefficient as will be shown subsequently. Between these two relatively stable regions is the region of inflation instability where the shock is alternately swallowed and expelled and the canopy is alternately inflated and partially collapsed. This region of inflation instability begins in the vicinity of the dashed line (fig. 17), which may be obtained from compressible flow tables and the following relationship between porosity and area ratio:

$$\frac{S_p}{S_v} = \frac{\left(\frac{2}{3}D_o\right)^2}{c_o D_o^2} = \frac{4}{9c_o}$$

The degree of inflation instability decreases steadily with increasing porosity until the upper stable region is reached where a normal shock is formed downstream of the canopy.

It may be noted that the stability regions are shown overlapping in figure 17 because their boundaries are difficult to establish. Variations in manufacturing techniques, gore patterns, canopy shape, and ribbon width undoubtedly affect these boundaries but it is believed only to a minor extent. Thus, it appears that porosity and Mach number are the most important factors which influence parachute stability.

The analysis does not take into account the effects of the wake caused by the body upstream, which will also affect parachute operation. However, in one test a small 90° cone (2 inches in diameter) was attached

to the riser line at the confluence point of the shroud lines of parachute 17 to see how this would affect parachute operation. The results may be seen in figure 18 and may be compared with results shown in figure 16(d) for the parachute without the small cone. Inflation instability occurred at a Mach number of 1.9 for both configurations of this parachute which had a porosity of 28.3 percent.

Several other observations may be made concerning stability of the parachutes listed in table II. Increasing porosity by means of a large center vent appears to be unsatisfactory. A low ribbon-spacing ratio b/B_{hr} is more satisfactory than a high ratio. Pulling in the center vent, as in parachute 12, gives some improvement in stability. The use of steel rods, or umbrella stays, to hold the parachute canopy open, as in parachute 17a, was unsatisfactory. The steel rods undoubtedly changed the effective porosity of the canopy and the altered shroud-line attachment proved to be unsatisfactory. The use of an inflatable ring at the canopy skirt to stiffen the parachute and prevent inflation instability was unsuccessful. This configuration exhibited the violent lateral oscillations characteristic of the low-porosity parachutes. However, this test was conducted at a Reynolds number of 750,000 per foot and tests of a similar configuration at the Lewis Research Center (ref. 2) indicated stable operation at high Reynolds numbers but unstable at low Reynolds numbers. Further research along these lines may be warranted, but the added weight of the ring and inflation apparatus may tend to offset the usual advantages of the parachute.

The cluster of three parachutes (number 11) was unstable and at times appeared to act as a single parachute undergoing inflation instability. This configuration is illustrated in figure 19.

Effect of porosity on drag coefficient.- Since the drag coefficients of parachutes are sometimes based on S_o and sometimes on S_p, both values are given in table II, III, and IV. However, in the discussion of results in this paper the drag coefficient referred to is that based on the projected, or frontal, area of a normally inflated parachute S_p which is calculated by using a diameter D_p two-thirds of the constructed, or laid-out-flat, diameter of the parachute.

In figure 20 the drag coefficients of the more stable flexible parachutes are plotted against constructed porosity in percent. Some of the data were obtained at a Mach number of 2.0 and some at a Mach number of 1.9. Omitted in the figure are the drag coefficients of parachutes 8 and 9, which were so unstable that an average drag coefficient may not be representative. Parachute 10, although more stable than parachutes 8 and 9, had a very low drag coefficient which is omitted in figure 20. The

reason for this low drag is not known. Also omitted is the drag coefficient of parachute 2, which was towed behind the Mercury capsule model, and parachute 12, which had a pulled-in center vent. The curve in figure 20 shows that drag coefficient decreases rapidly with increasing porosity at a Mach number of 2.0. The data at a Mach number of 1.9 were obtained on parachutes having a porosity which placed them in the region of inflation instability at a Mach number of 1.9. This is believed to be the reason for the scatter of the data at this Mach number, for it is quite difficult to measure drag accurately when the parachute is operating in the region of inflation instability. The region of violent oscillations from side to side and up and down, where no data could be obtained, is indicated in figure 20 for a Mach number of 2.0.

Effect of Mach number and payload on drag coefficient.- The variation of drag coefficient with Mach number for parachutes 1 and 2 is shown in figure 21. The drag of these parachutes when towed behind the Mercury capsule model is compared in figure 21(a) and the drag of parachute 1 when towed behind the conical-nosed cylindrical body is compared in figure 21(b) with its drag when towed behind the Mercury capsule model. The curves in figure 21 show a characteristic rise in drag coefficient with Mach number until a critical value is reached at a Mach number of about 2, after which the drag coefficient decreases rapidly. This rapid decrease in average drag coefficient is caused by the onset of inflation instability. Figure 21(a) shows that this decrease in drag coefficient with increase in Mach number is less for parachute 2, which was slightly larger in diameter than parachute 1. However, when parachute 1 was towed behind the conical-nosed cylindrical body, its maximum drag coefficient was considerably lower and occurred at a lower Mach number than when towed behind the Mercury capsule. This difference indicates that the wake from the parachute's payload had considerable effect on its drag coefficient. The tow-cable length during these tests was 10.7 times the payload base diameter.

Effect of parachute reefing on drag coefficient.- The variation of drag coefficient with parachute opening in percent of the nominal diameter is shown in figure 22 for a Mach number of 2.0. The data for parachute openings up to 40 percent were taken from table IV and the value of drag coefficient for a normally inflated parachute $\left(\frac{2}{3}D_o\right)$ with a porosity of 28 percent was taken from the curve in figure 20. Figure 22 shows that reefing is an effective means of modulating the drag of parachutes at supersonic speeds. This technique will reduce the snatch loads during deployment and, by using an automatic disreefing device (ref. 7), the drag may be increased as the velocity of the payload decreases because of the drag force.

Rotochute model.- No significant results were obtained in tests of the rotochute model but some observations may be made concerning operation of such a parachute. The high-speed schlieren motion picture shows a characteristic rotary motion of the tow cable which is caused by the rotating parachute. The center of the rotating parachute appears to be a node, with an antinode, or loop, at the confluence point of the shroud lines. Attempts were made to eliminate this antinode by shortening the tow cable and also by extending the shroud lines to a disk (free to rotate) at the base of the payload. However, the rotochute failed in each case before any results could be obtained. It appears that considerable development work will be required on this type of rotochute.

CONCLUSIONS

An investigation has been made to determine the parameters affecting the aerodynamic performance of drogue parachutes in the Mach number range from 1.6 to 3. The following conclusions may be made:

1. Porosity and Mach number are the most important factors influencing the drag and stability of flexible porous parachutes. Such parachutes have a limited range of stable operation at supersonic speeds, except for those with very high porosities, but the drag coefficient decreases rapidly with increasing porosity.

2. For a parachute with 20-percent porosity there is a characteristic rise in drag coefficient with Mach number until a critical value is reached at a Mach number of about 2, after which the drag coefficient decreases rapidly because of inflation instability.

3. The wake from the parachute's payload had considerable effect on the parachute drag coefficient when the tow-cable length was 10.7 times the payload base diameter.

4. Reefing is an effective means of modulating the drag of parachutes at supersonic speeds.

5. A low ribbon-spacing ratio results in more satisfactory operation than a high ratio. Increasing porosity by means of a large center vent appears to be unsatisfactory.

6. The use of mechanical means of stiffening a parachute canopy to prevent inflation instability does not appear promising.

Langley Research Center,
National Aeronautics and Space Administration,
Langley Field, Va., January 18, 1961.

REFERENCES

1. Wiant, Harry W., and Fredette, Raymond O.: A Study of High Drag Configurations as First Stage Decelerators. WADC Tech. Note 56-320, U.S. Air Force, July 1956.

2. Connors, James F., and Lovell, J. Calvin: Some Observations on Supersonic Stabilization and Deceleration Devices. Paper No. 60-19, Inst. Aero. Sci., Jan. 1960.

3. Bowman, James S., Jr.: Dynamic Model Tests at Low Subsonic Speeds of Project Mercury Capsule Configurations With and Without Drogue Parachutes. NASA TM X-459, 1961.

4. Johnson, Clinton T.: Investigation of the Characteristics of 6-Foot Drogue-Stabilization Ribbon Parachutes at High Altitudes and Low Supersonic Speeds. NASA TM X-448, 1960.

5. Anon.: Manual for Users of the Unitary Plan Wind Tunnel Facilities of the National Advisory Committee for Aeronautics. NACA, 1956.

6. Meyer, R. A.: Wind Tunnel Investigation of Conventional Types of Parachute Canopies in Supersonic Flow. WADC Tech. Rep. 58-532, U.S. Air Force, Dec. 1958.

7. Lafferty, J. F., and Lange, K. O.: The University of Kentucky Continuous Disreefing Device. WADC Tech. Note 58-177, U.S. Air Force, May 1959.

TABLE I.- CHARACTERISTICS OF RIGID-PARACHUTE MODELS

Configuration		Angle of attack, deg	Mach number	Dynamic pressure, lb/sq ft	Flow characteristics
Canopy I: Poroxity, 20 percent; no center vent	Without shroud lines	0	2.30	200	Unsteady
		0	2.98	200	Unsteady
		0	3.50	200	Unsteady
		0	3.71	200	Unsteady
	24 shroud lines 12 in. long	0	1.57	200	Unsteady
		0	1.87	200	Unsteady
		0	2.16	200	Unsteady
		0	2.30	200	Unsteady
		0	2.98	200	Unsteady
		0	3.71	200	Unsteady
		1	2.16	200	Unsteady
	24 shroud lines 24 in. long	0	2.98	200	Unsteady
		0	3.20	100	Unsteady
		0	3.71	200	Unsteady
Canopy II: Porosity, 24 percent; no center vent	Without shroud lines	0	3.00	200	Unsteady
		0	3.04	200	Unsteady
		0	3.60	125	Unsteady
		0	3.60	150	Unsteady
		0	3.70	140	Unsteady
		0	3.90	115	Unsteady
		1	3.35	150	Unsteady
		4	3.90	115	Unsteady
Canopy III: Porosity, 35 percent; center-vent diameter, 1.14 in.	Without shroud lines	0	1.70	250	Steady
		5	1.70	180	Steady
Canopy IV: Porosity, 45 percent; center-vent diameter, 5.714 in.	Without shroud lines	0	2.30	190	Steady
		0	3.00	250	Steady
		0	3.50	160	Steady
	24 shroud lines 24 in. long	0	2.65	210	Unsteady
		0	2.65	182	Unsteady
		0	2.65	166	Unsteady
		0	2.40	187	Unsteady
		0	3.00	250	Unsteady
		0	3.50	160	Unsteady
	24 shroud lines 12 in. long	0	2.30	190	Unsteady
		0	3.00	250	Unsteady
		0	3.50	160	Unsteady
	12 shroud lines 12 in. long	0	1.77	290	Unsteady
		0	2.17	240	Unsteady
		0	2.30	190	Unsteady
		0	2.76	155	Unsteady
		0	3.00	250	Unsteady
		0	3.50	160	Unsteady
	6 shroud lines 12 in. long	0	1.77	290	Unsteady
		0	2.17	240	Unsteady
		0	2.76	155	Unsteady
		2	2.76	155	Unsteady
	6 shroud lines 12 in. long with flow stabilizers	0	2.76	155	Unsteady
		0	2.76	100	Unsteady
Canopy V: Porosity, 36.5 percent; center-vent diameter, 4.326 in.	Without shroud lines	0	1.70	300	Steady
Canopy VI: Porosity, 28 percent; center-vent diameter, 2.448 in.	Without shroud lines	0	1.77	290	Steady
		0	2.17	240	Steady

TABLE II.- CHARACTERISTICS OF FLEXIBLE PARACHUTE MODELS

Parachute number	Nominal diameter, ft	Porosity, percent	Number of shroud lines	Total area, S_o, sq ft	Gore details in figure	Photograph in figure	Mach number	Dynamic pressure, lb/sq ft	Reynolds number per ft	C_D based on S_o	C_D based on S_p	Remarks
1	0.600	20.0	8	0.283	5(a)	4(a)	2.00	153	0.687×10^6	0.294	0.661	Stable
1a	.600	1.0	8	.283	*	4(b)	3.10	*	*	*	*	Very unstable; failed
2	.800	19.0	12	.502	5(b)	4(c)	2.00	153	.685	.328	.738	Towed behind model of Mercury capsule; stable
3	1.250	19.0	12	1.227	*	4(d)	3.10	*	*	*	*	Very unstable; failed
4	.500	50.0	8	.196	*	4(e)	2.00	154	.691	*	*	Parachute made of net; shroud line failed
5	.833	60.0	8	.545	*	4(f)	2.00	154	.691	.108	.244	Not fully inflated, but fairly stable
6	1.000	50.0	8	.785	*	4(g)	2.00	154	.692	.137	.308	Not fully inflated, but fairly stable
7	.667	83.0	8	.349	*	4(h)	2.00	154	.691	.059	.134	Not fully inflated, but quite stable
8	.950	40.5	8	.708	5(c)	*	1.90	162	.715	.113	.254	Large center vent; unstable
9	.950	33.8	8	.708	5(d)	4(i)	1.90	155	.683	.099	.223	Large center vent; unstable
10	.950	20.0	8	.708	5(e)	*	1.90	165	.729	.105	.236	Normal center vent; fairly stable
11	.512	20.0	8	.206	*	*	1.90	172	*	*	*	Cluster of three parachutes; unstable
12	.950	20.0	8	.708	*	*	1.90	170	.748	.180	.405	Pulled-in center vent; partially stable
13	.824	29.0	16	.532	5(f)	*	1.90	166	.731	.272	.612	Partially stable
14	.992	25.0	16	.770	5(g)	*	1.90	163	.720	.217	.488	Fairly stable
15	.925	28.5	16	.671	5(h)	*	1.90	164	.722	.257	.578	Partially stable
15a	.925	28.5	16	.671	5(h)	4(j)	2.85	140	.750	*	*	Inflatable ring in canopy skirt; very unstable; failed
16	.815	28.3	16	.520	5(i)	*	1.90	161	.708	.224	.504	45° conical canopy; fairly stable
17	.924	28.3	16	.670	5(j)	*	1.90	175	.754	.241	.542	30° conical canopy; fairly stable
17a	.924	28.3	8	.670	5(j)	4(k)	2.00	*	*	*	*	Canopy stiffened by steel rods; unstable

*Not available.

TABLE III.- TEST CONDITIONS FOR PARACHUTES 1 AND 2

Configuration	Mach number	Dynamic pressure, lb/sq ft	Reynolds number per ft	C_D based on S_o	C_D based on S_p
Parachute 1 towed behind conical-nosed cylindrical body	1.60	180	0.796×10^6	0.265	0.596
	1.82	168	.742	.305	.686
	2.00	153	.687	.294	.661
	2.25	132	.612	.245	.551
	2.37	121	.577	.233	.524
	2.50	109	.537	.193	.435
Parachute 1 towed behind Mercury capsule	1.82	171	0.755×10^6	0.333	0.748
	2.00	154	.687	.386	.868
	2.25	133	.618	.254	.572
	2.50	109	.535	.214	.482
Parachute 2 towed behind Mercury capsule	1.82	173	0.761×10^6	0.285	0.642
	2.00	153	.684	.328	.738
	2.25	148	.688	.282	.635
	2.50	109	.533	.247	.556

TABLE IV.- TEST CONDITIONS FOR REEFED PARACHUTE

[Nominal diameter, D_o, 1.73 ft; porosity, 28 percent]

Parachute opening, percent of D_o	Mach number	Dynamic pressure, lb/sq ft	Reynolds number per ft	C_D based on S_o	C_D based on S_p
12.5	1.80	284	1.25×10^6	0.034	0.077
12.5	2.00	258	1.15	.040	.090
12.5	2.20	228	.99	.043	.097
25.0	1.80	284	1.25×10^6	0.067	0.151
25.0	2.00	258	1.15	.063	.142
25.0	2.20	228	.99	.062	.139
25.0	2.87	138	.70	.056	.126
33.3	1.80	284	1.25×10^6	0.067	0.151
33.3	2.00	258	1.15	.066	.148
33.3	2.20	228	.99	.067	.151
33.3	2.87	138	.70	.071	.160
40.0	1.80	284	1.25×10^6	0.097	0.218
40.0	2.00	258	1.15	.094	.211
40.0	2.20	228	.99	.089	.198

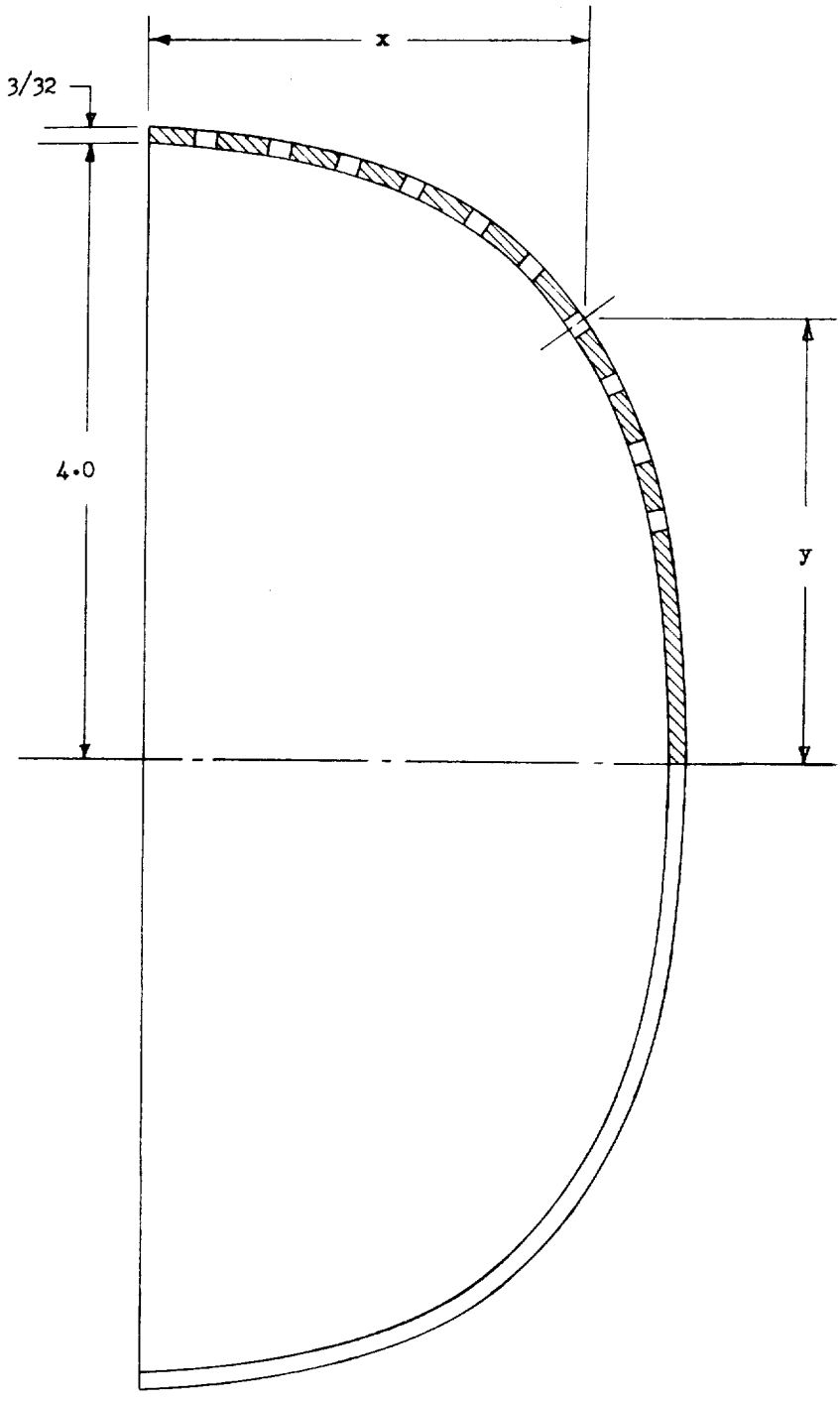

Canopy Ordinates	
x	y
0	4.093
.384	4.076
.867	4.001
1.294	3.910
1.735	3.758
2.153	3.535
2.510	3.234
2.824	2.859
3.062	2.485
3.248	2.046
3.370	1.584
3.500	0

Figure 1.- Details of rigid-parachute-canopy shape. All dimensions are in inches.

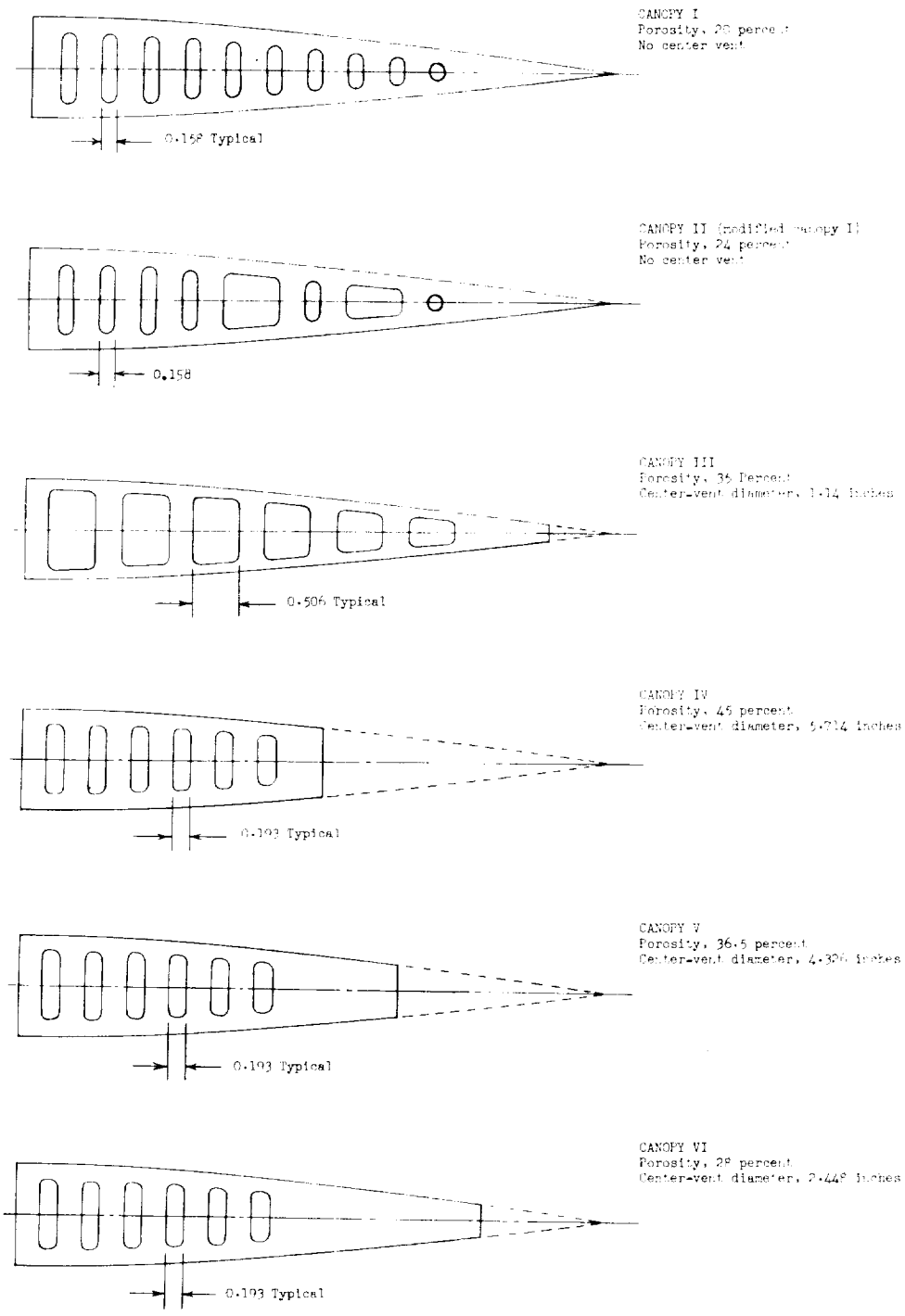

Figure 2.- Gore layouts for the various 24-gore rigid-canopy models tested. All dimensions are in inches.

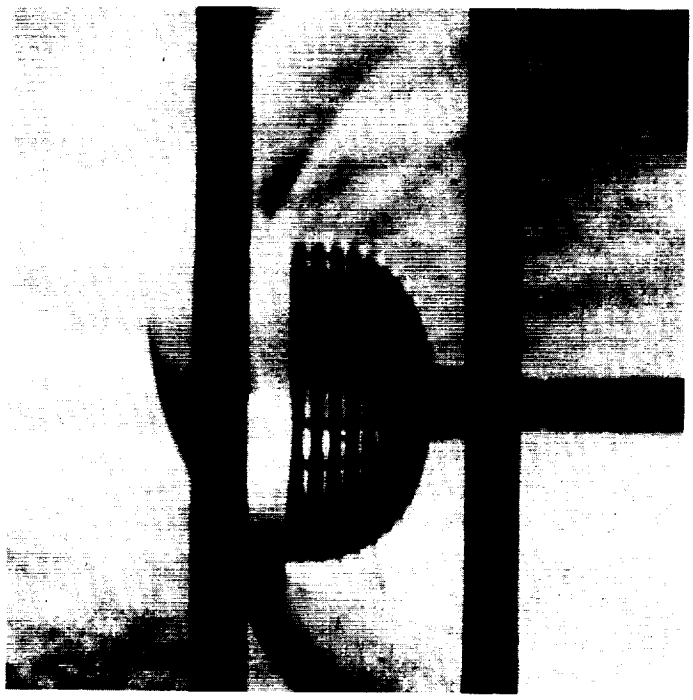

(a) Schlieren photograph showing sting support used in tests of canopies I and II having no center vent. M = 2.3.

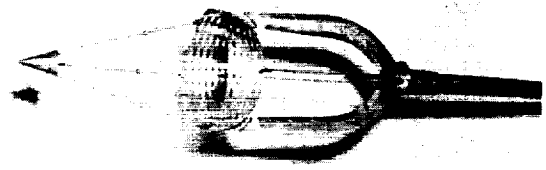

(b) Photograph of sting support used in tests of canopies III, IV, V, and VI having center vents. L-61-36

Figure 3.- Sting supports used in tests of rigid-parachute-canopy models.

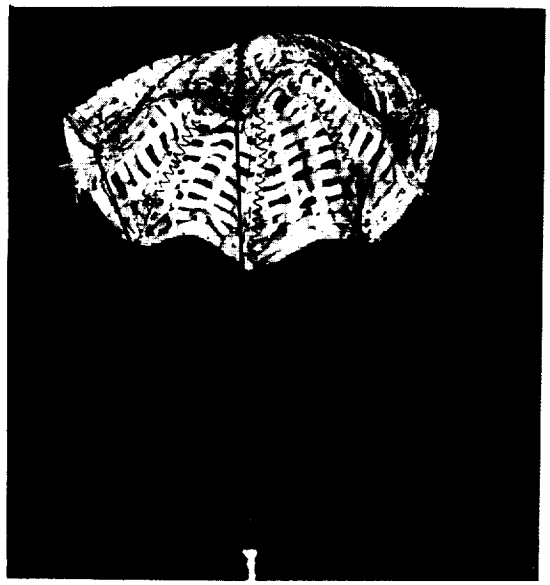

(a) Parachute 1.

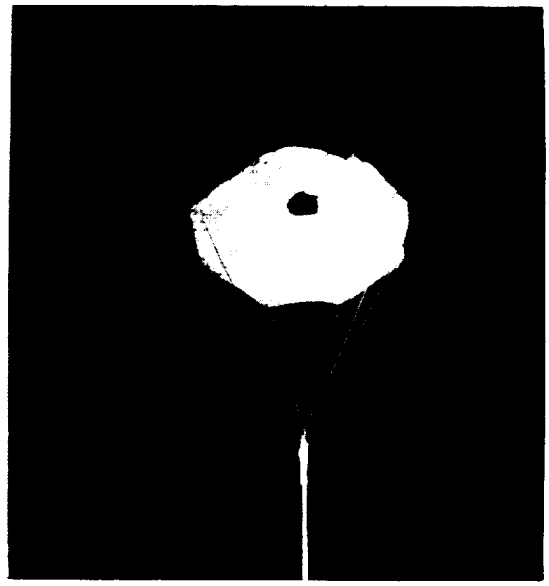

(b) Parachute 1a.

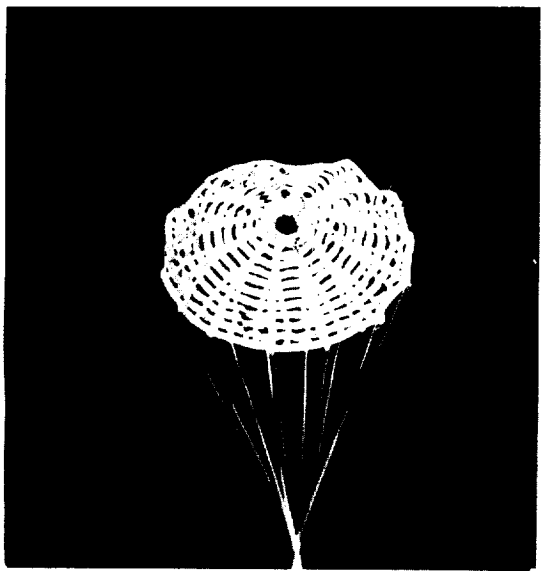

(c) Parachute 2.

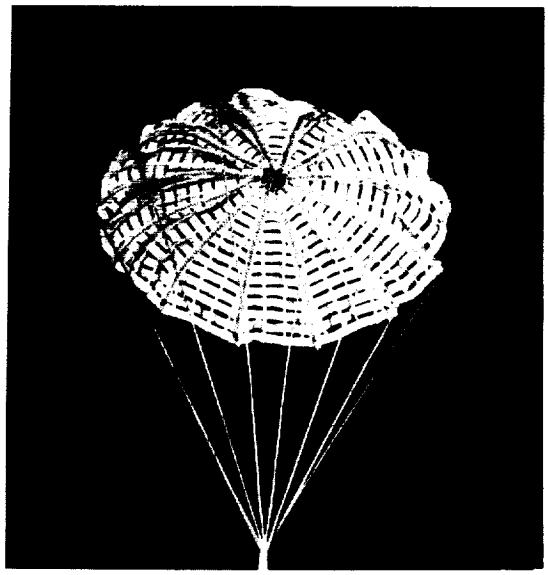

(d) Parachute 3. L-61-48

Figure 4.- Photographs of flexible-parachute models.

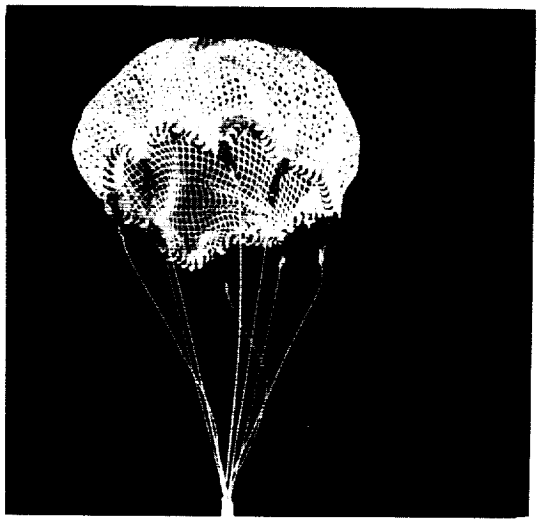

(e) Parachute 4.

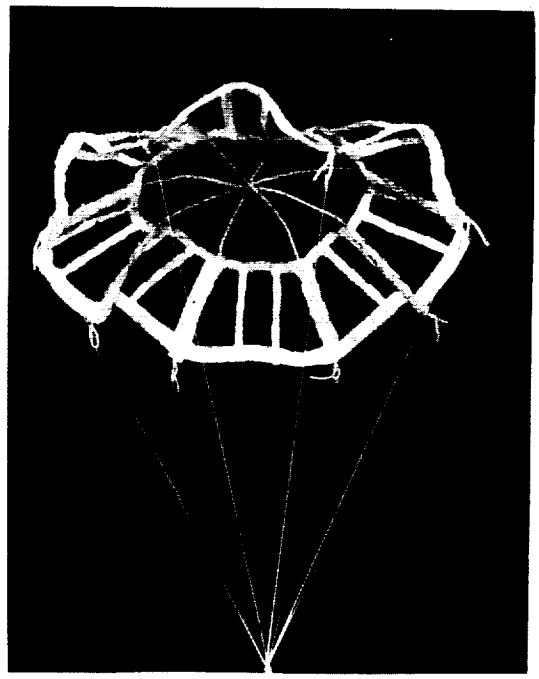

(f) Parachute 5.

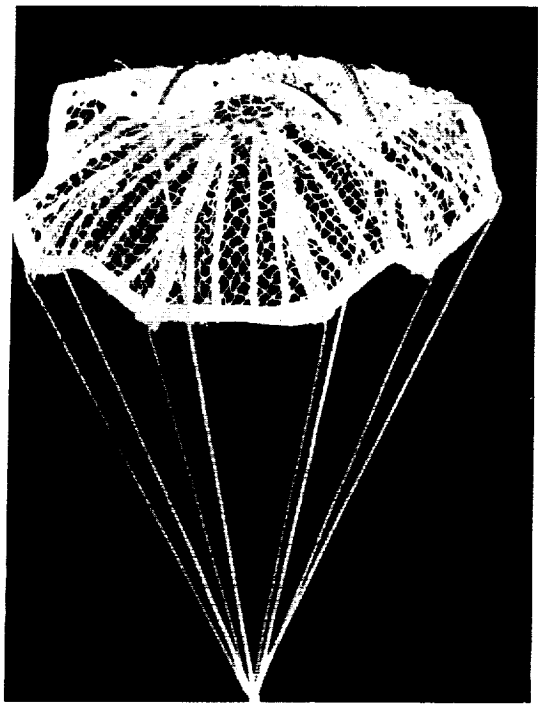

(g) Parachute 6.

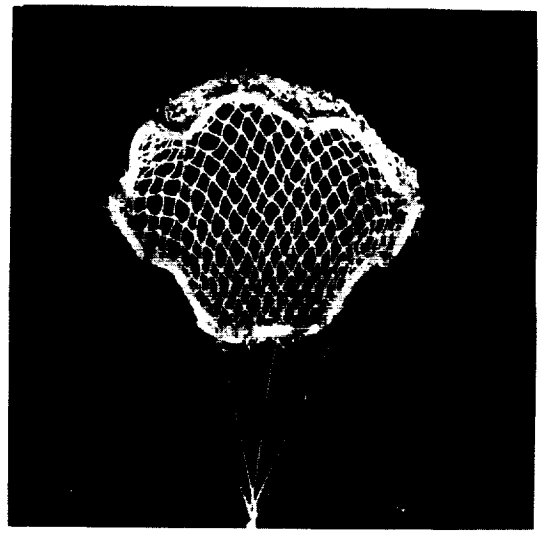

(h) Parachute 7. L-61-49

Figure 4.- Continued.

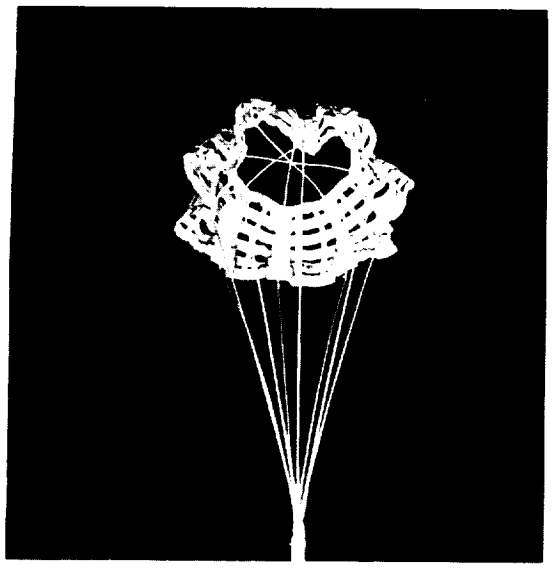

(i) Parachute 9.

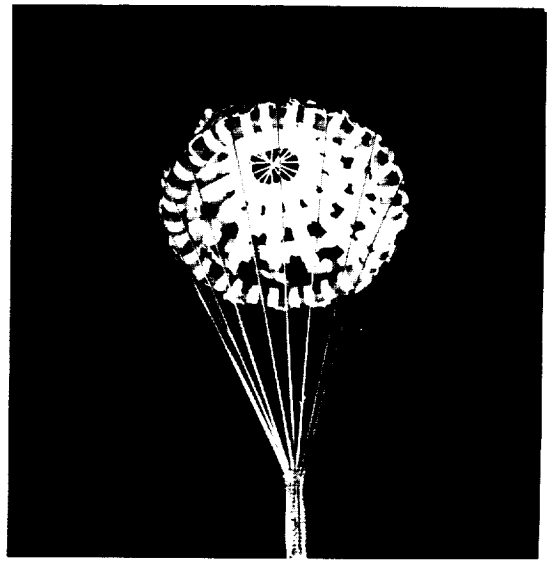

(j) Parachute 15a.

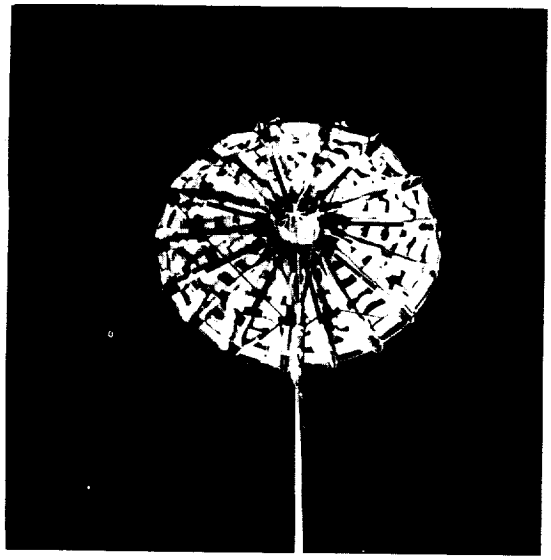

(k) Parachute 17a.

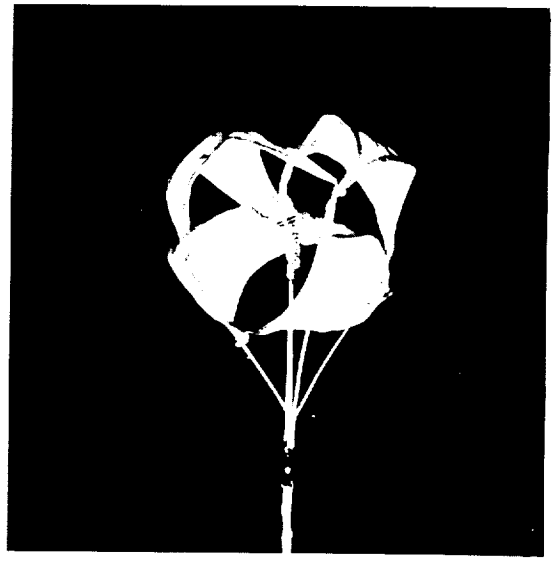

(l) Rotochute. L-61-50

Figure 4.- Concluded.

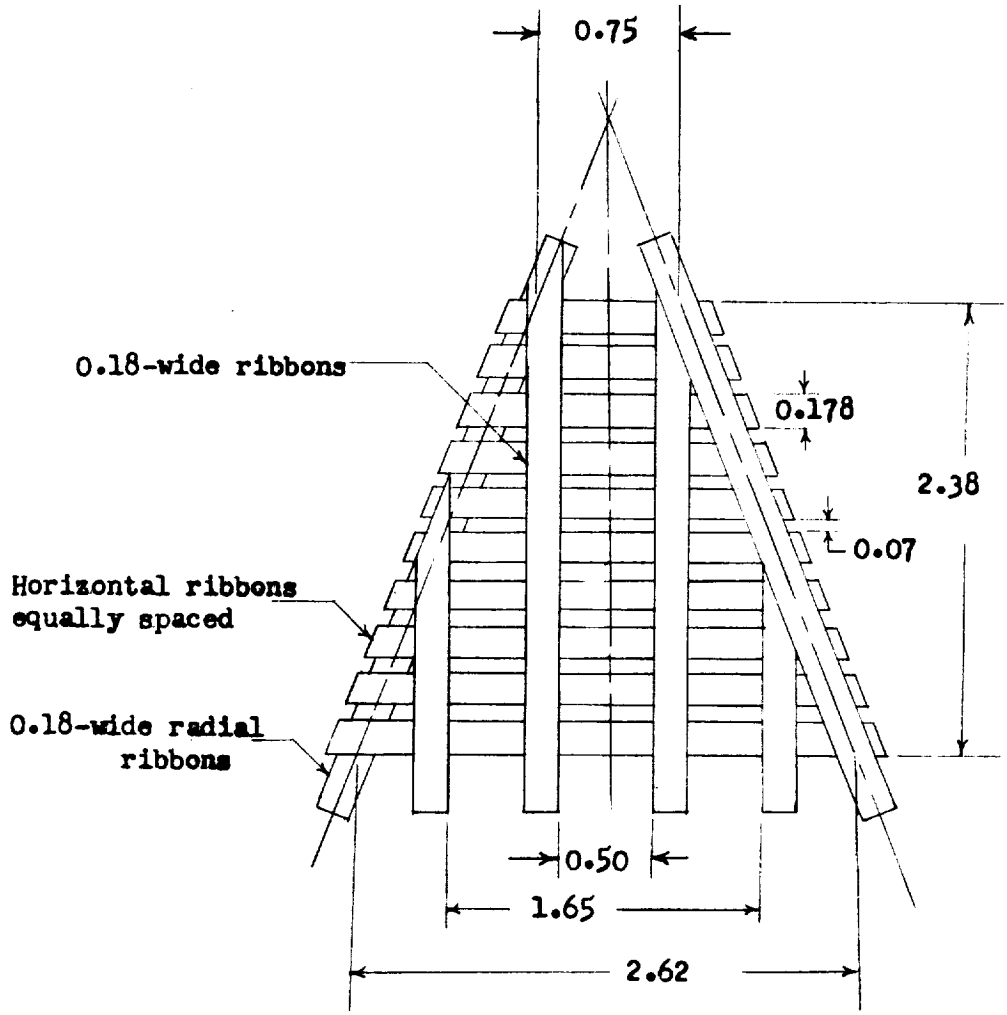

(a) Parachute 1.

Figure 5.- Gore details of flexible-parachute models. All dimensions are in inches.

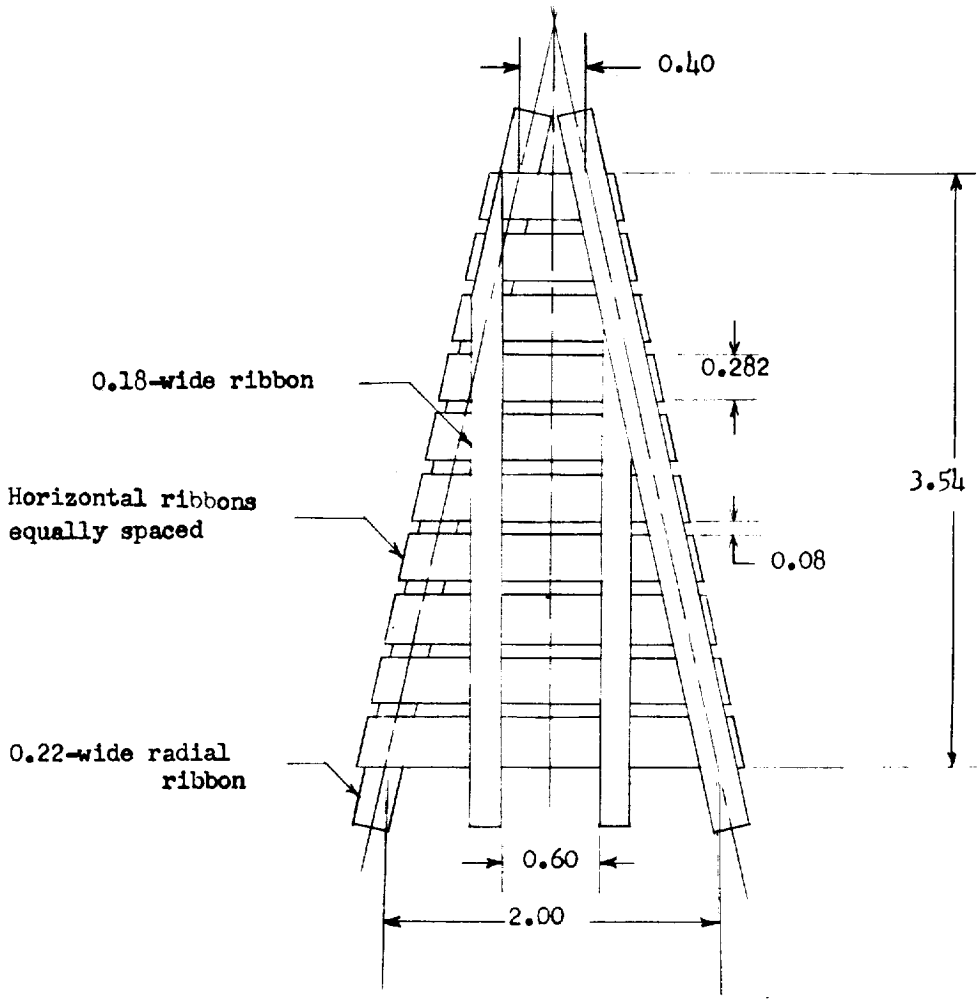

(b) Parachute 2.

Figure 5.- Continued.

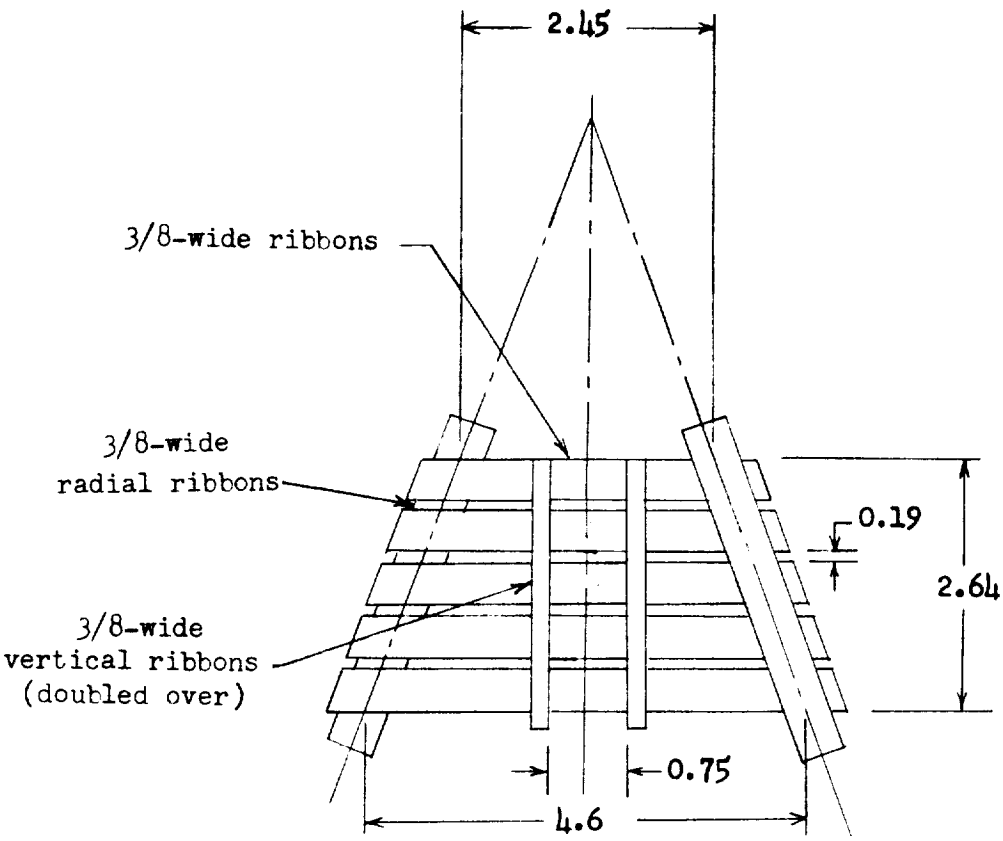

(c) Parachute 8.

Figure 5.- Continued.

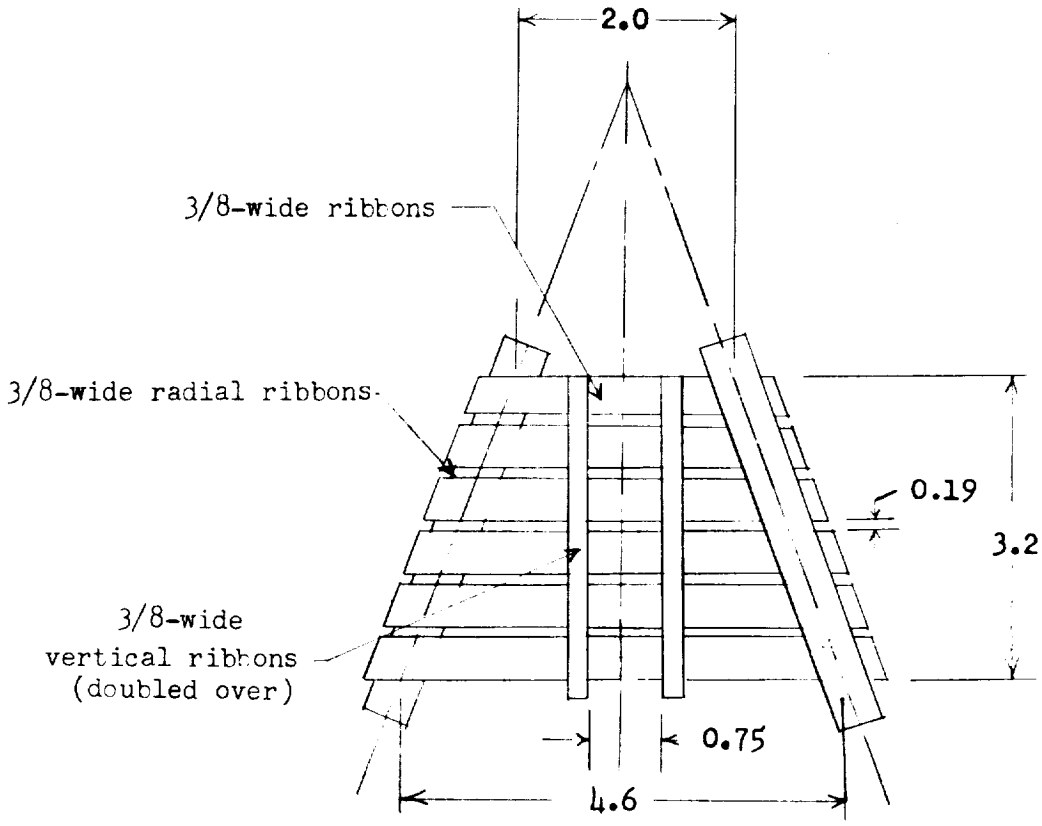

(d) Parachute 9.

Figure 5.- Continued.

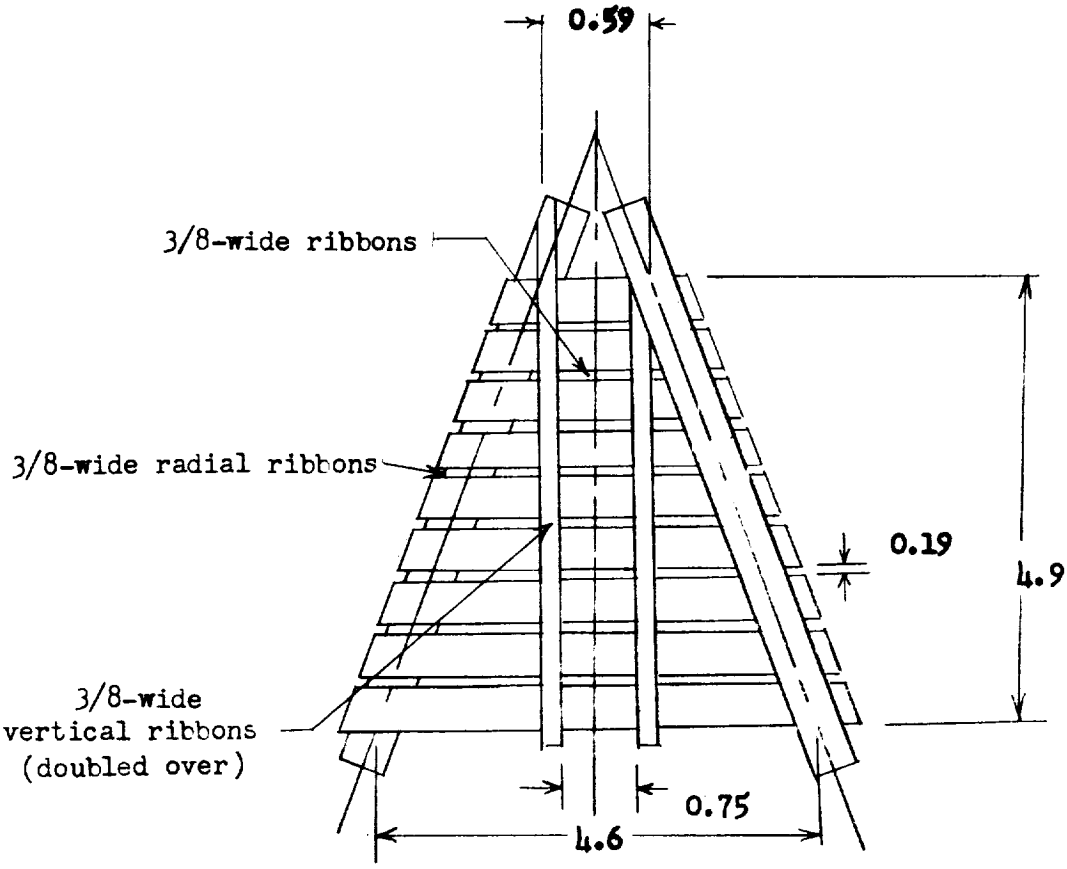

(e) Parachute 10.

Figure 5.- Continued.

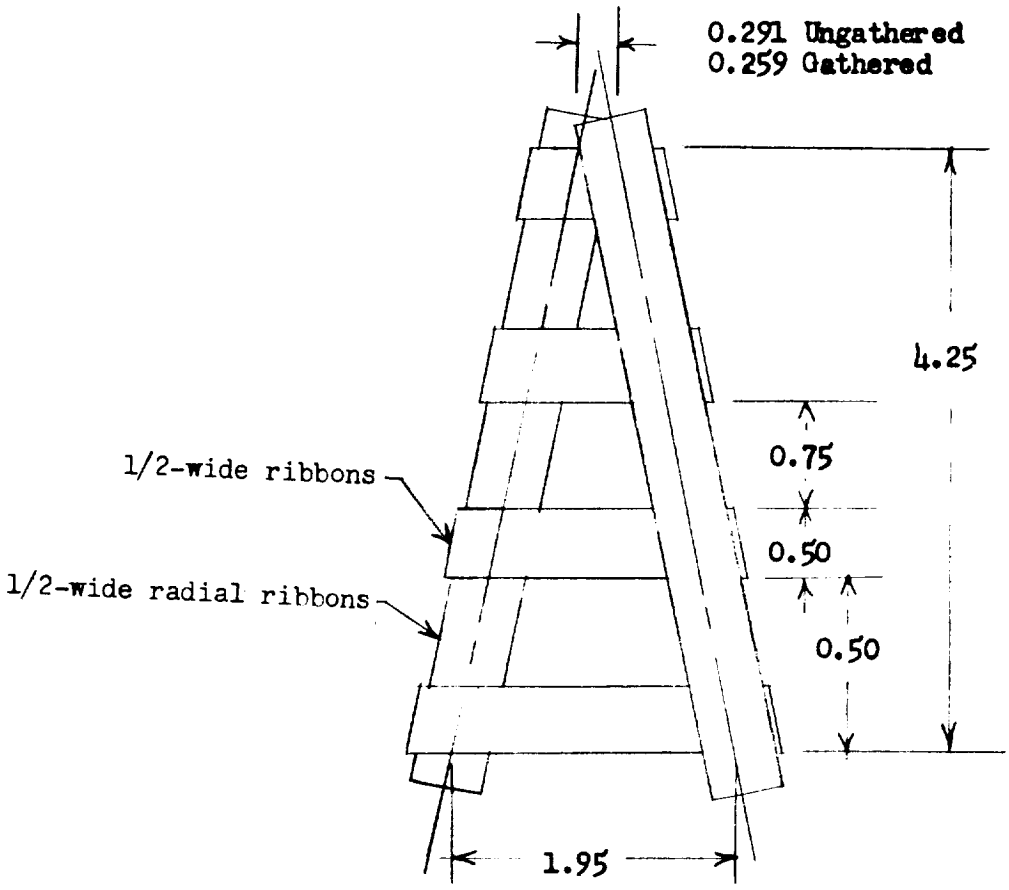

(f) Parachute 13.

Figure 5.- Continued.

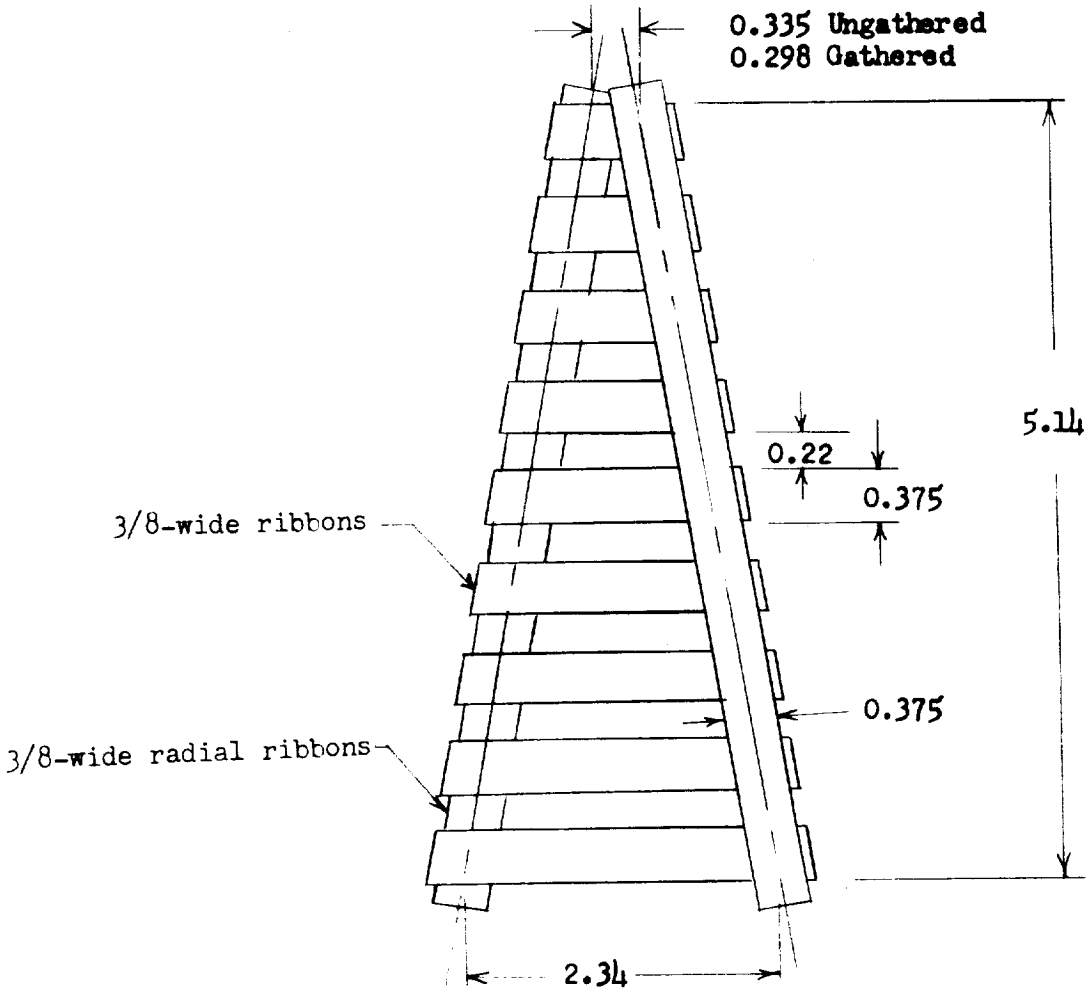

(g) Parachute 14.

Figure 5.- Continued.

L-723

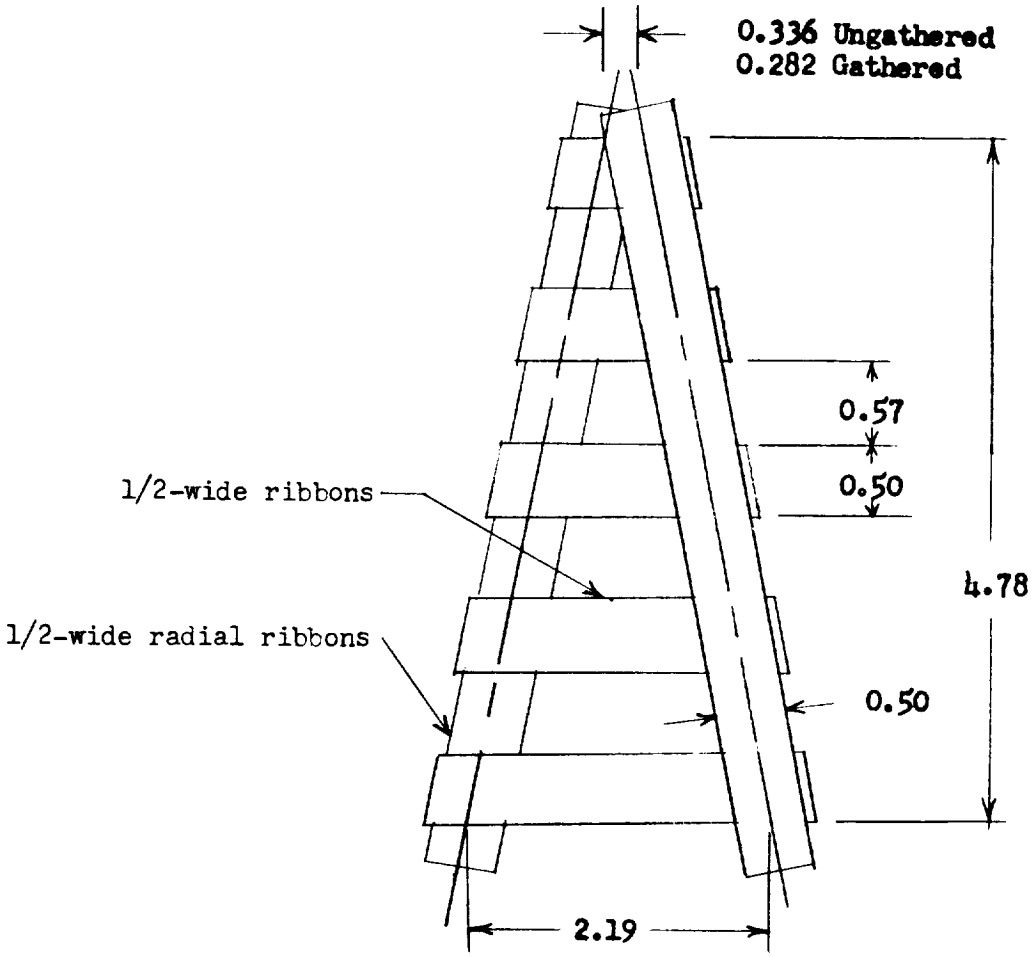

(h) Parachutes 15 and 15a.

Figure 5.- Continued.

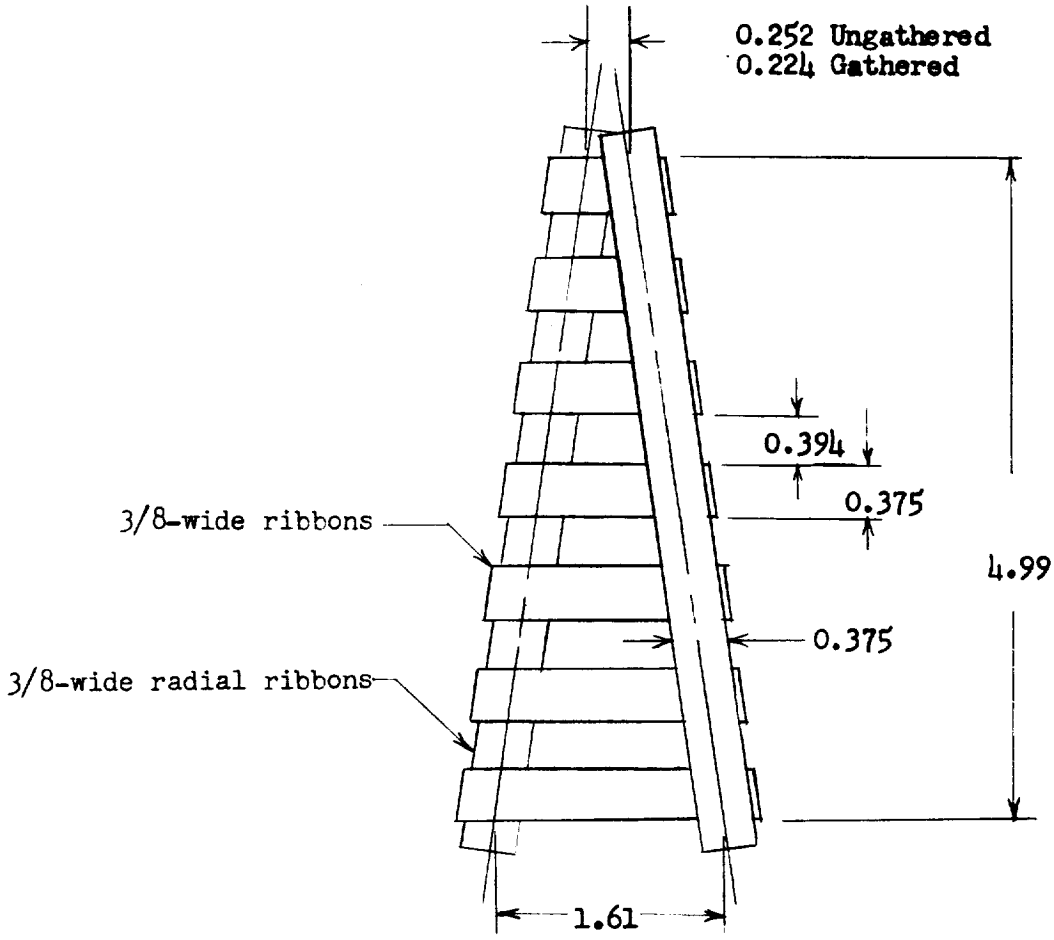

(i) Parachute 16.

Figure 5.- Continued.

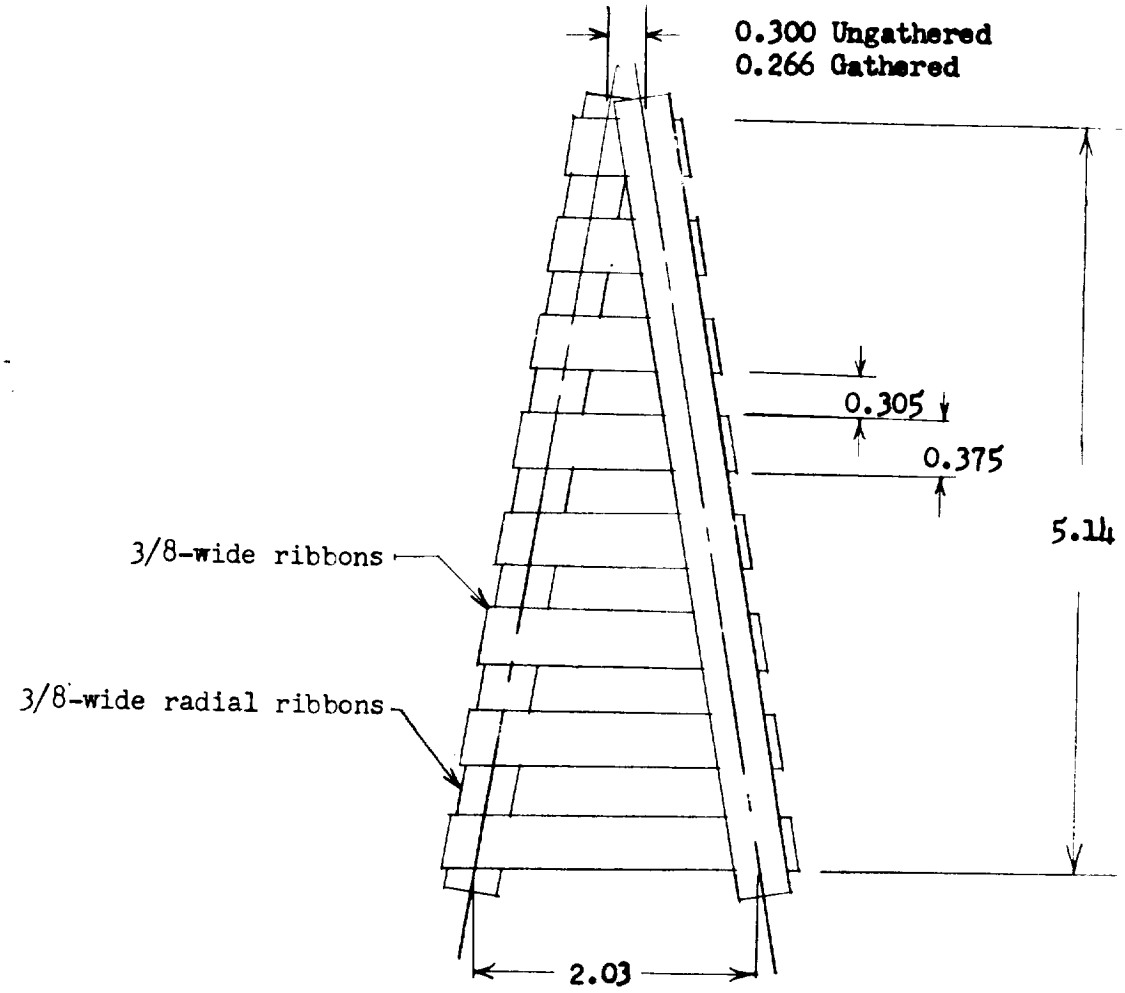

(j) Parachutes 17 and 17a.

Figure 5.- Concluded.

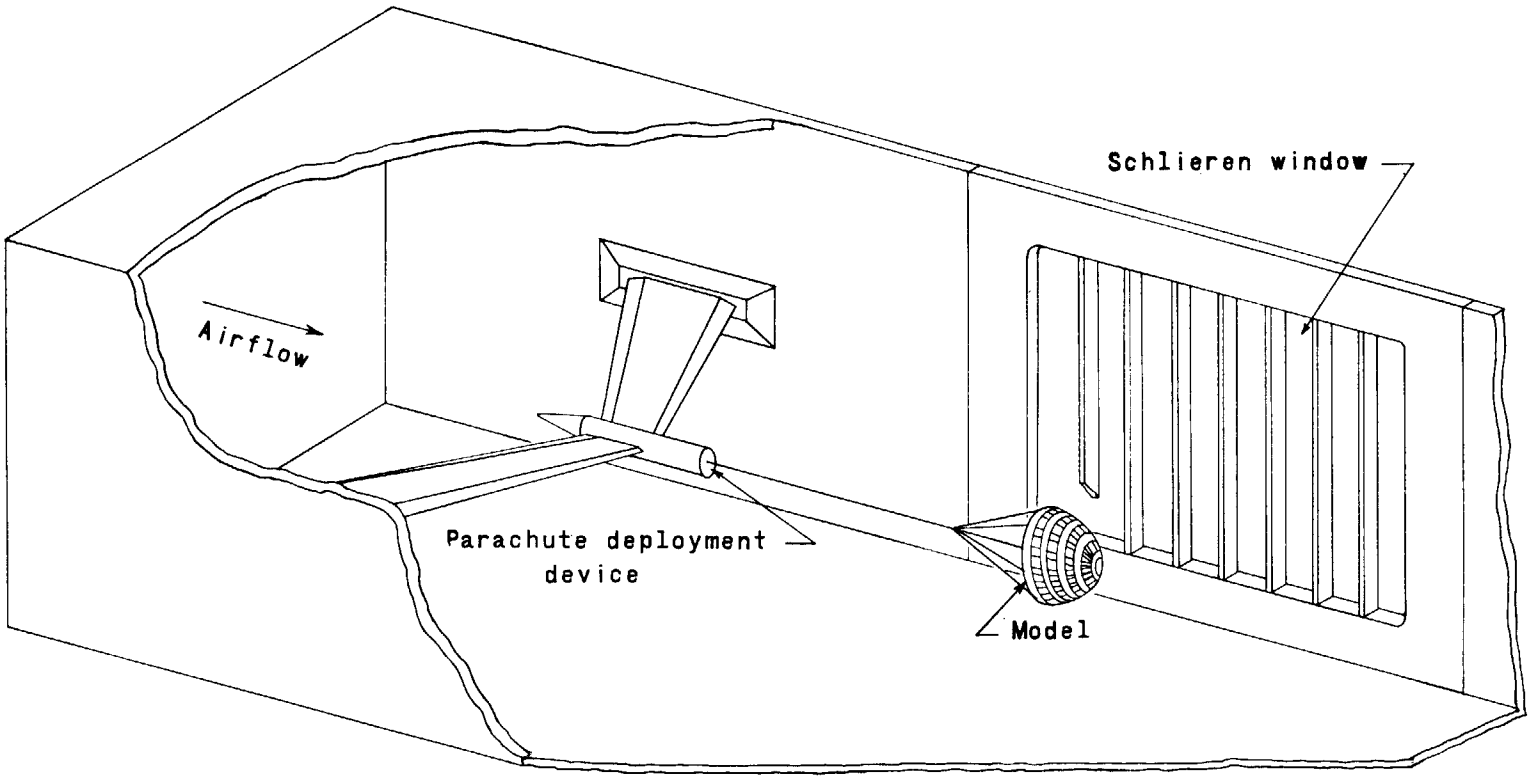

Figure 6.- Sketch of conical-nosed cylindrical body mounted on support struts for tests of drogue parachutes.

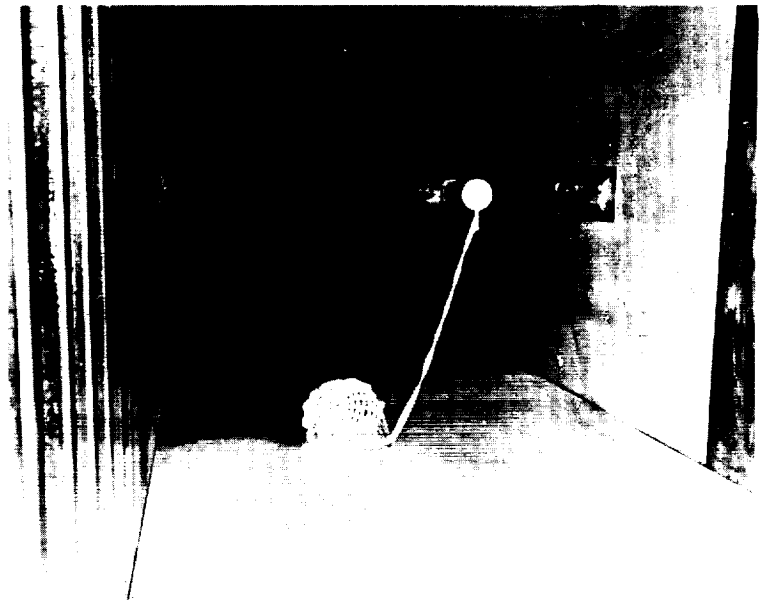

(a) Looking upstream. L-59-342

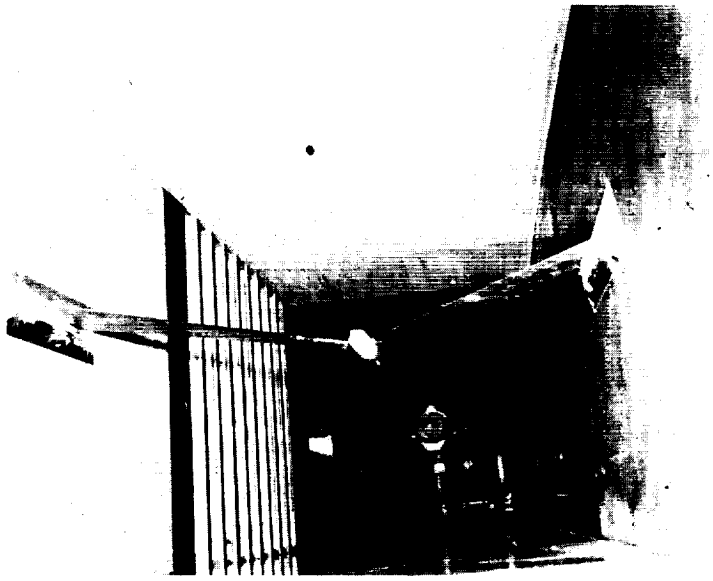

(b) Looking downstream. L-59-339

Figure 7.- Photographs of conical-nosed cylindrical body mounted on support struts for tests of drogue parachutes.

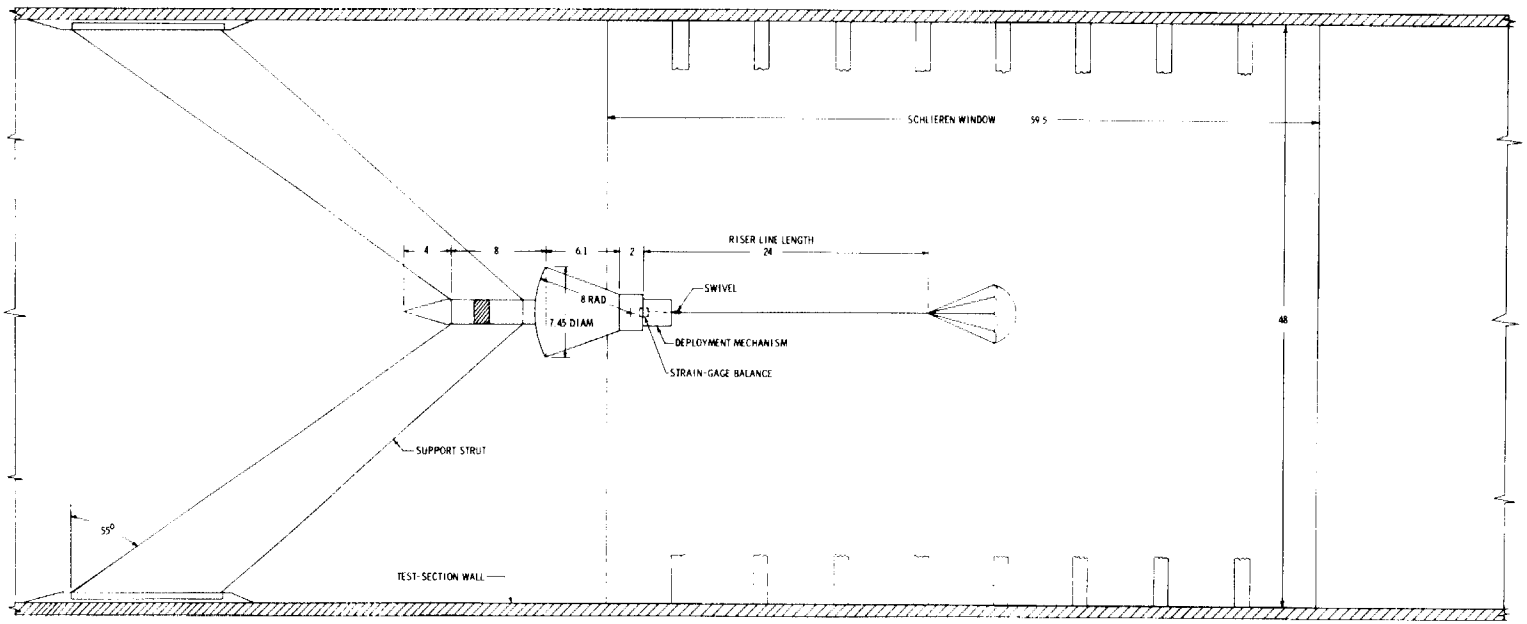

Figure 8.- Sketch of 1/10-scale model of Mercury capsule mounted in Langley Unitary Plan wind tunnel for tests of drogue parachutes. All dimensions are in inches.

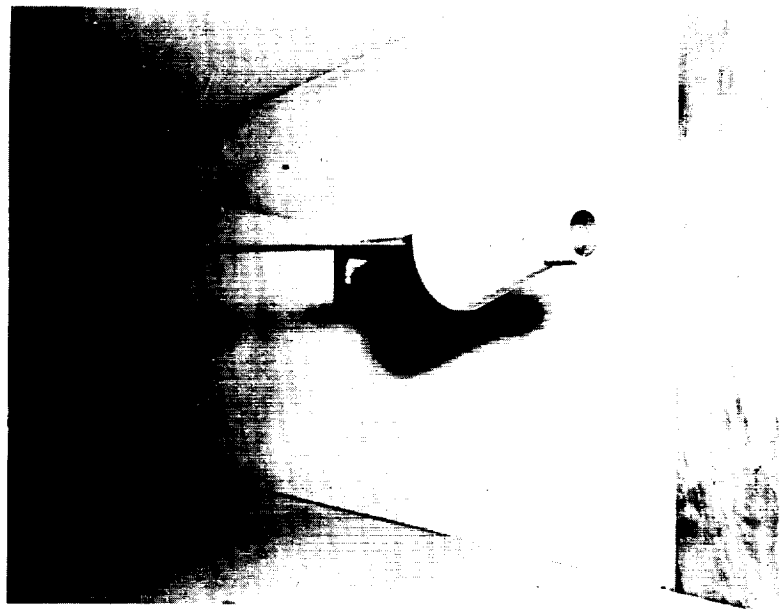

L-723

(a) Looking upstream. L-59-5491

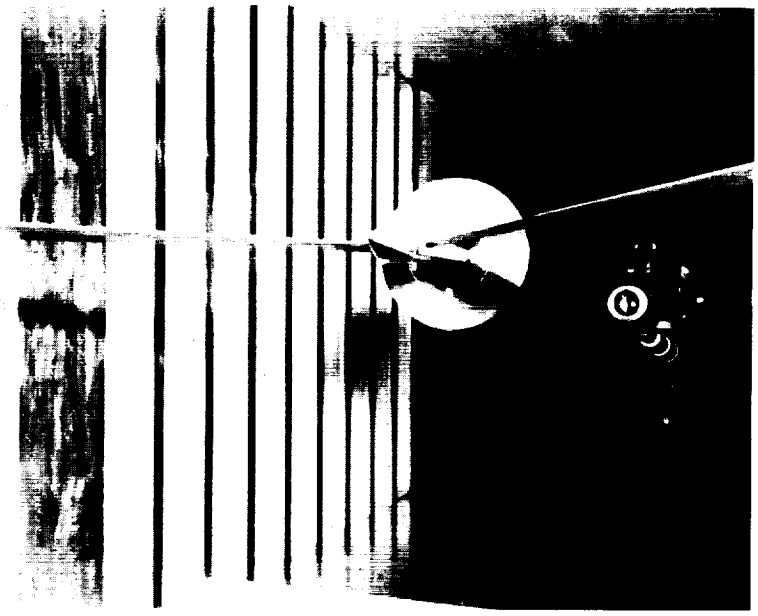

(b) Looking downstream. L-59-5492

Figure 9.- Photographs of 1/10-scale model of Mercury capsule mounted on support struts for tests of drogue parachutes.

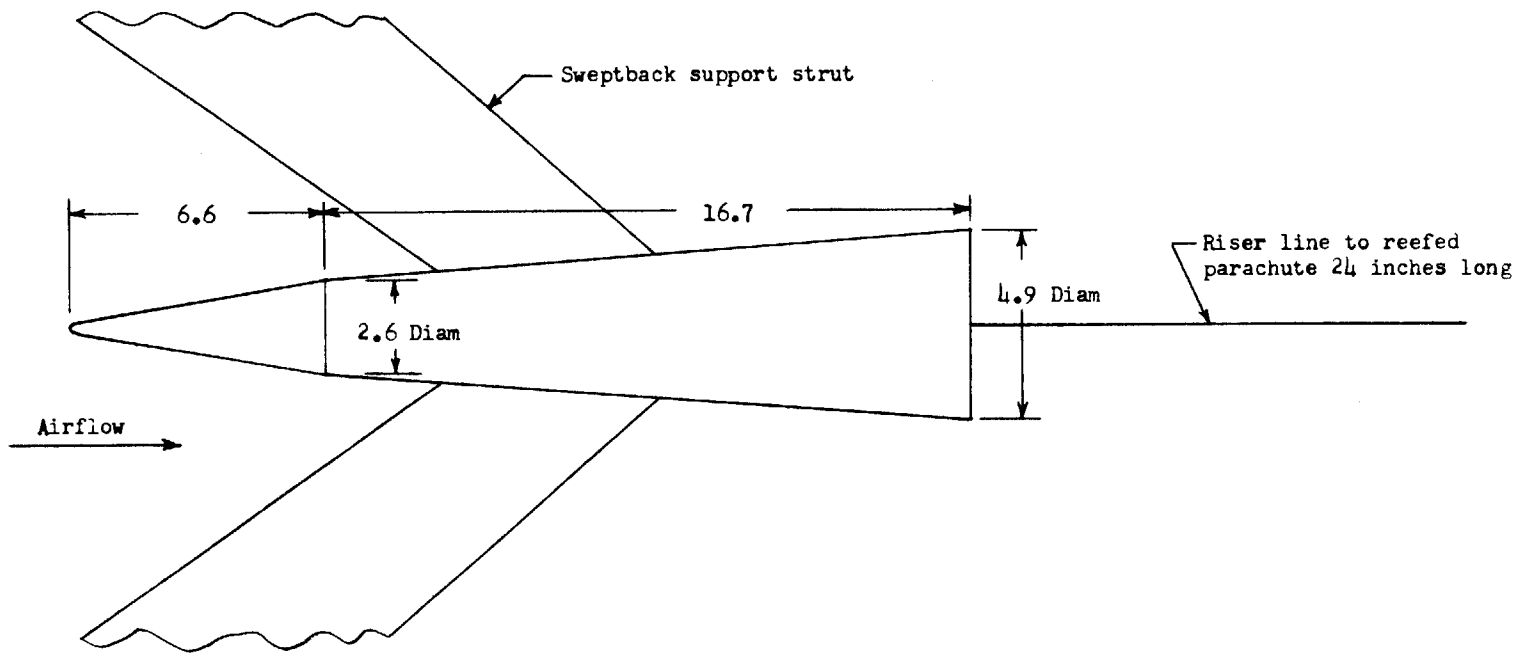

Figure 10.- Sketch of conical body used in tests of reefed parachute. All dimensions are in inches.

L-61-37

Figure 11.- Schlieren photographs showing change in shock pattern with time for a rigid-parachute canopy without shroud lines. Canopy porosity, 20 percent; Mach number, 2.3; dynamic pressure, 200 lb/sq ft.

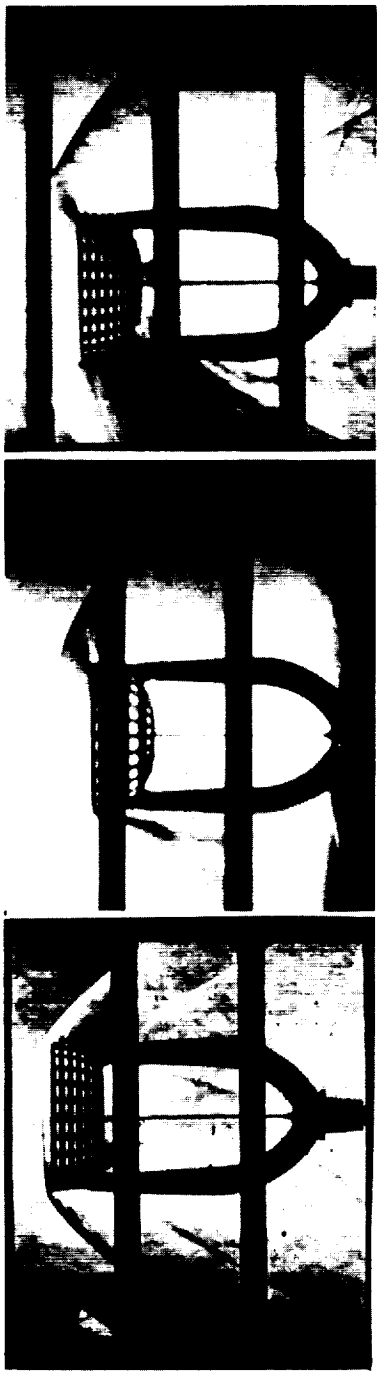

(a) Canopy porosity, 28 percent. Mach number, 1.77; dynamic pressure, 290 lb/sq ft.

(b) Canopy porosity, 35 percent. Mach number, 1.70; dynamic pressure, 250 lb/sq ft.

(c) Canopy porosity, 45 percent. Mach number, 2.30; dynamic pressure, 190 lb/sq ft.

L-723

L-61-38

Figure 12.- Schlieren photographs showing the steady shock pattern obtained on rigid-parachute canopies without shroud lines.

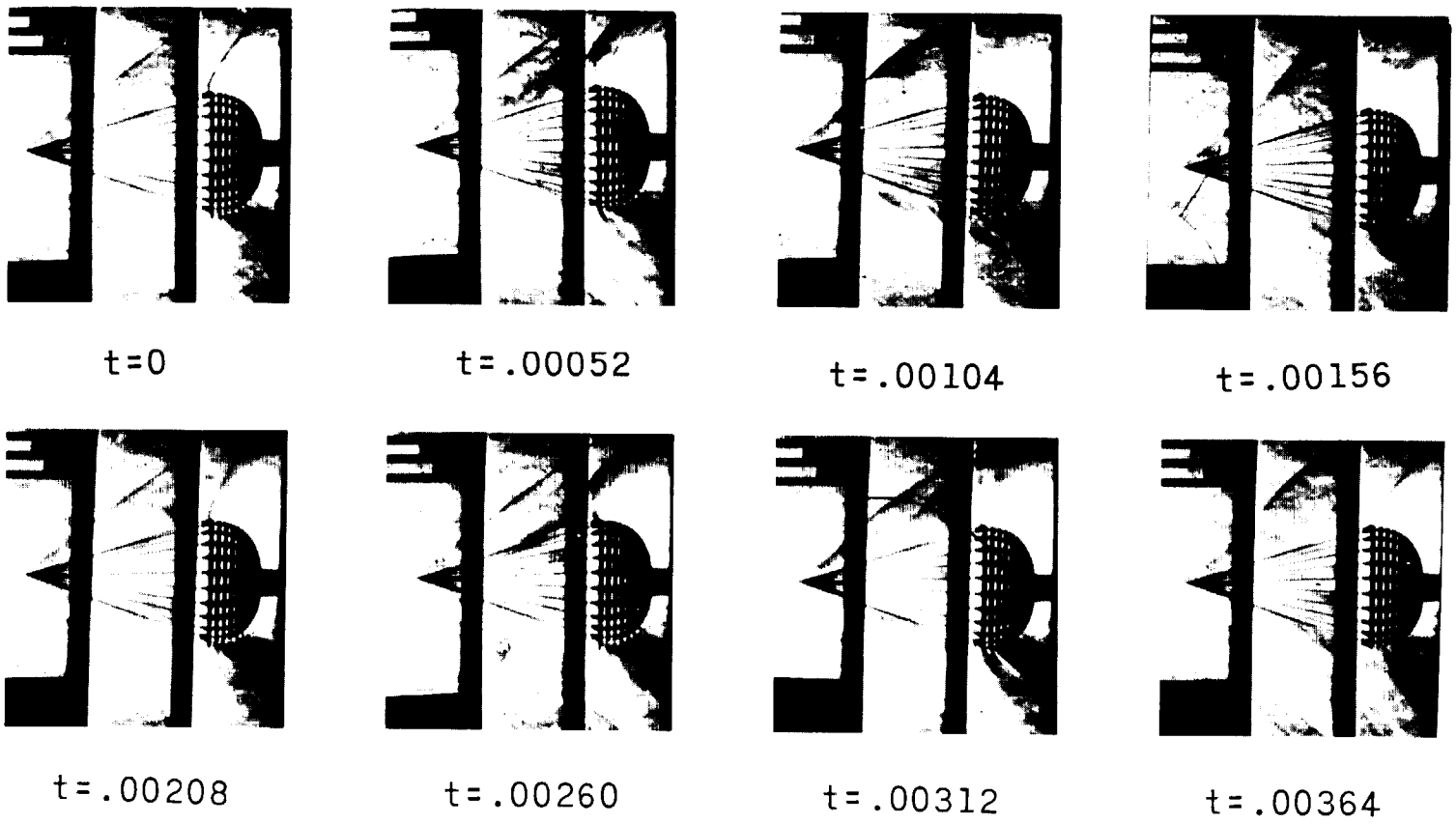

L-61-39

Figure 13.- Schlieren photographs showing the change in shock pattern with time for a rigid parachute canopy with 24 shroud lines 1 foot in length. Canopy porosity, 20 percent; Mach number, 1.87; dynamic pressure, 200 lb/sq ft.

(a) 12 shroud lines.

(b) 6 shroud lines. L-61-40

Figure 14.- Schlieren photographs showing effect of number of shrouds on shock pattern of a rigid parachute canopy with shrouds 1 foot in length. Canopy porosity, 45 percent; Mach number, 1.77; dynamic pressure, 290 lb/sq ft.

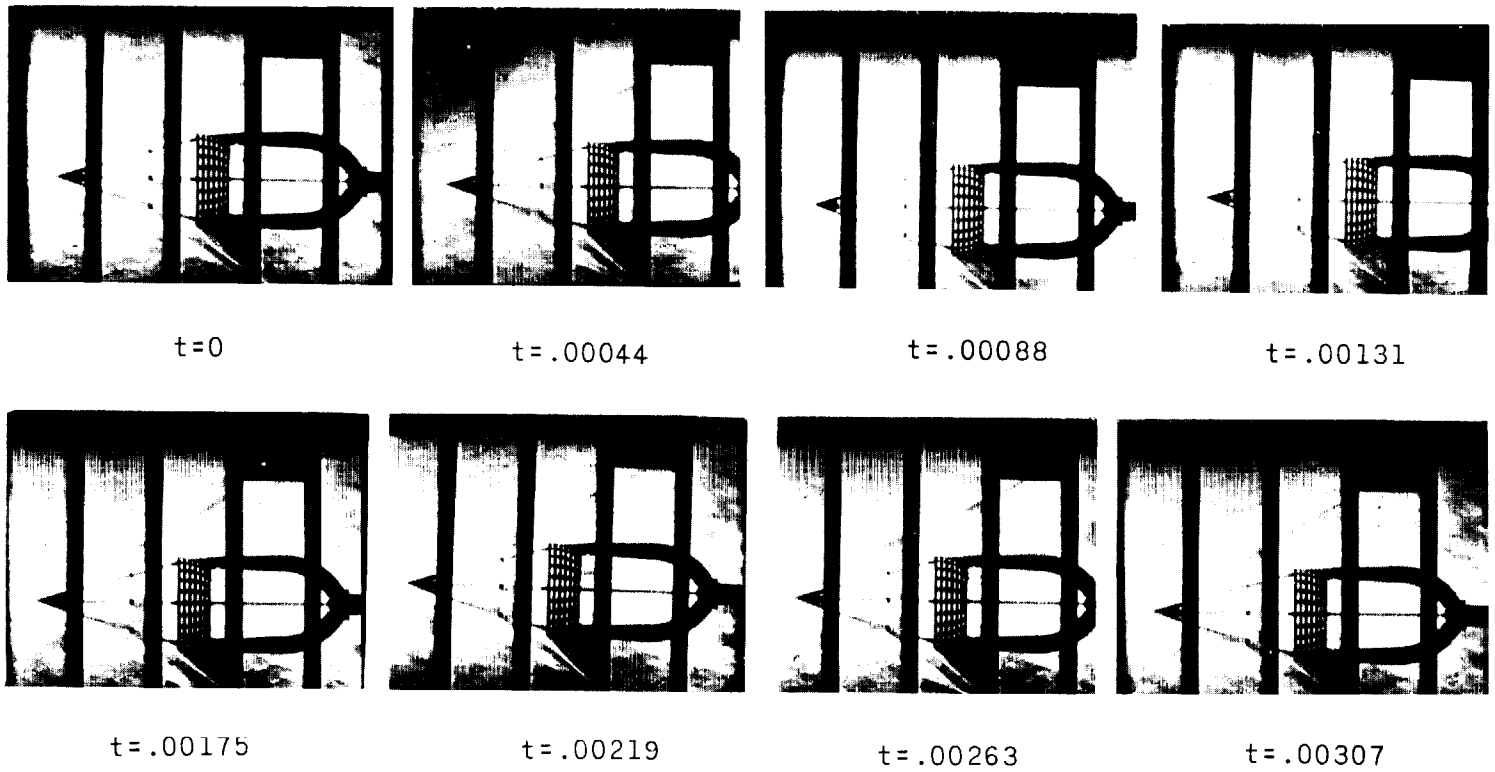

L-61-41

Figure 15.- Schlieren photographs showing change in shock pattern with time for a rigid parachute canopy with six shroud lines 1 foot in length and with flow stabilizers 4 inches upstream of canopy skirt. Canopy porosity, 45 percent; Mach number, 2.76; dynamic pressure, 100 lb/sq ft.

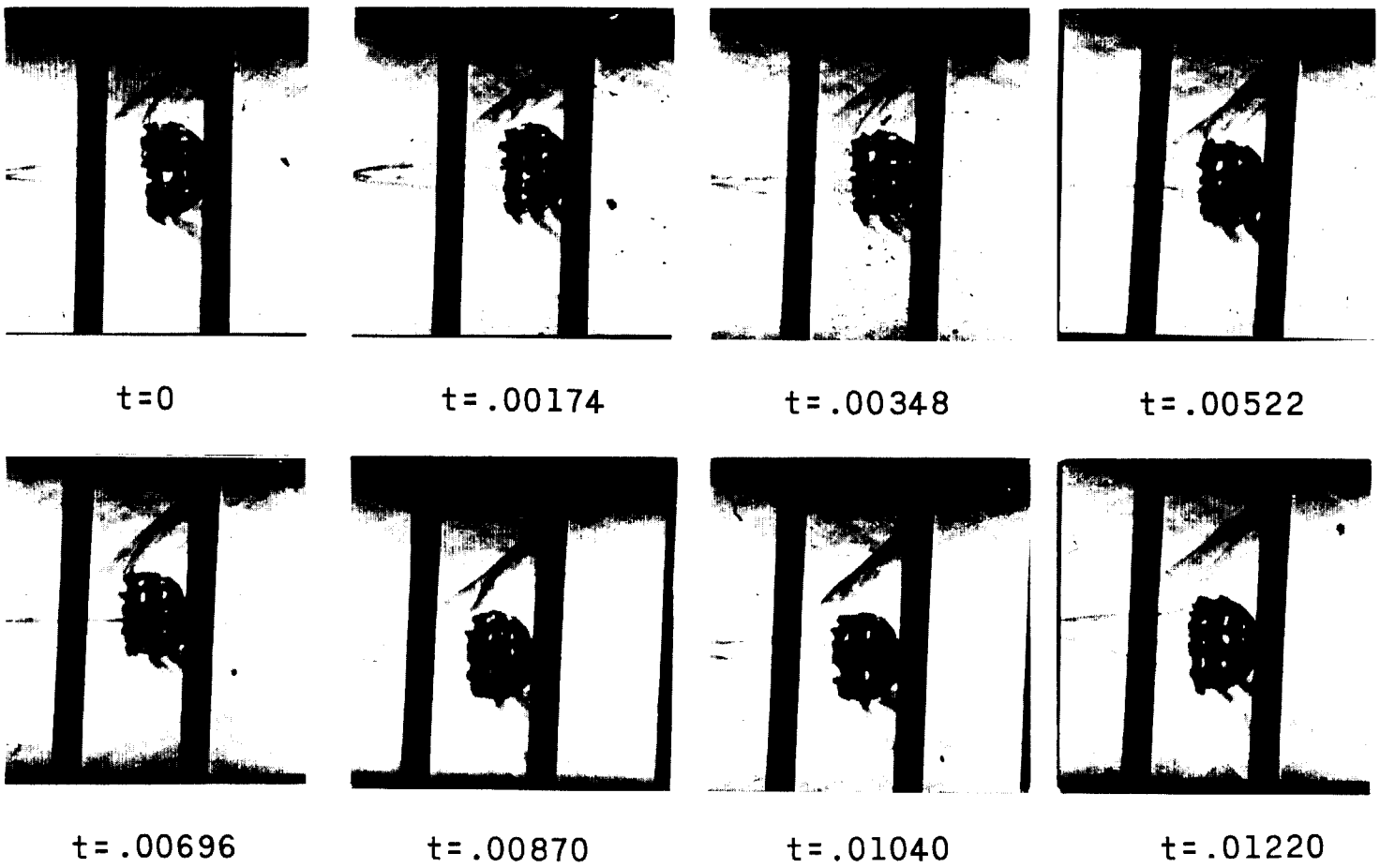

(a) Parachute 13. Mach number, 1.90; dynamic pressure, 166 lb/sq ft. L-61-42

Figure 16.- Schlieren photographs showing change in shock pattern with time for several flexible-parachute models.

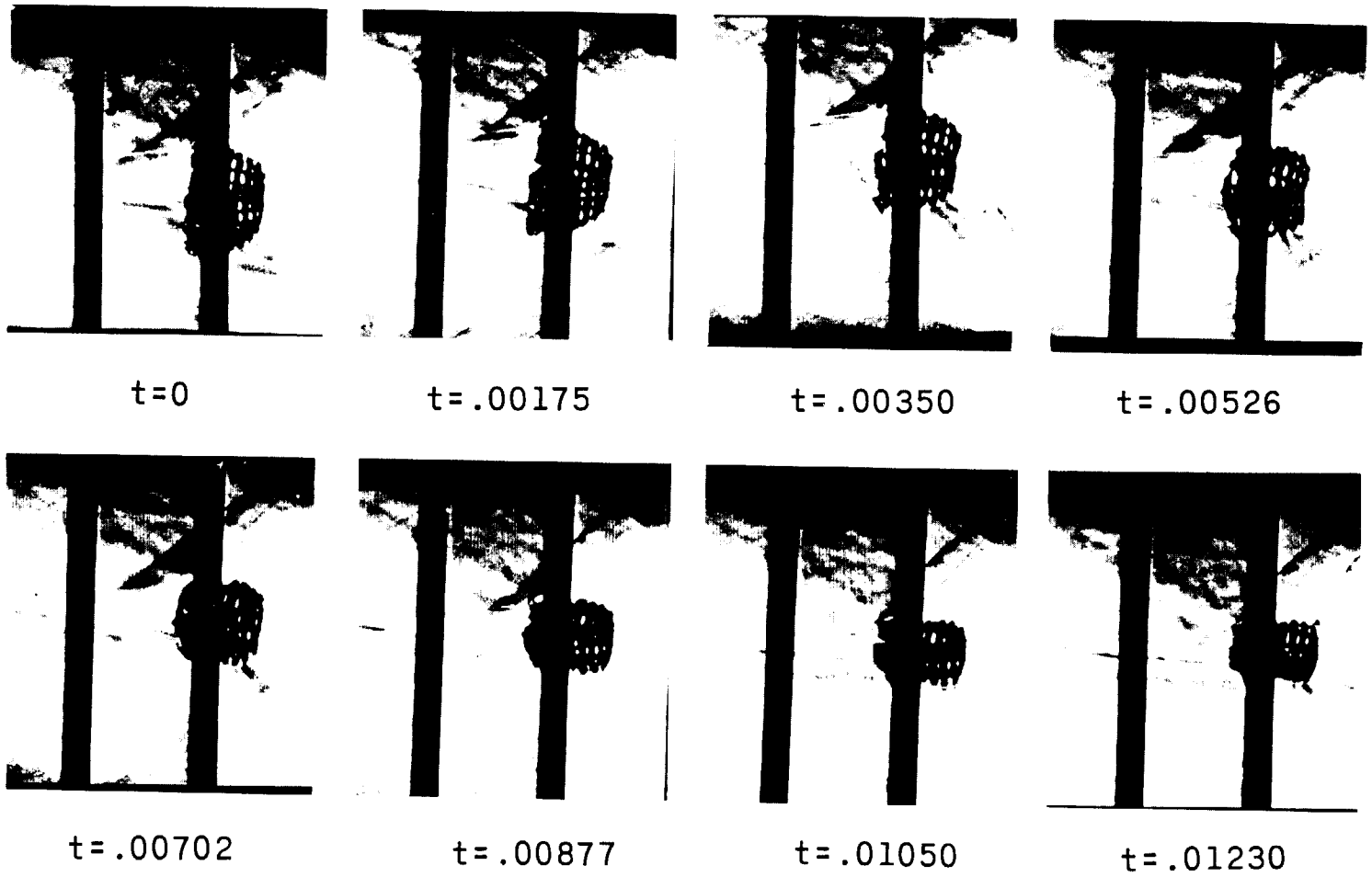

(b) Parachute 14. Mach number, 1.90; dynamic pressure, 163 lb/sq ft. L-61-43

Figure 16.- Continued.

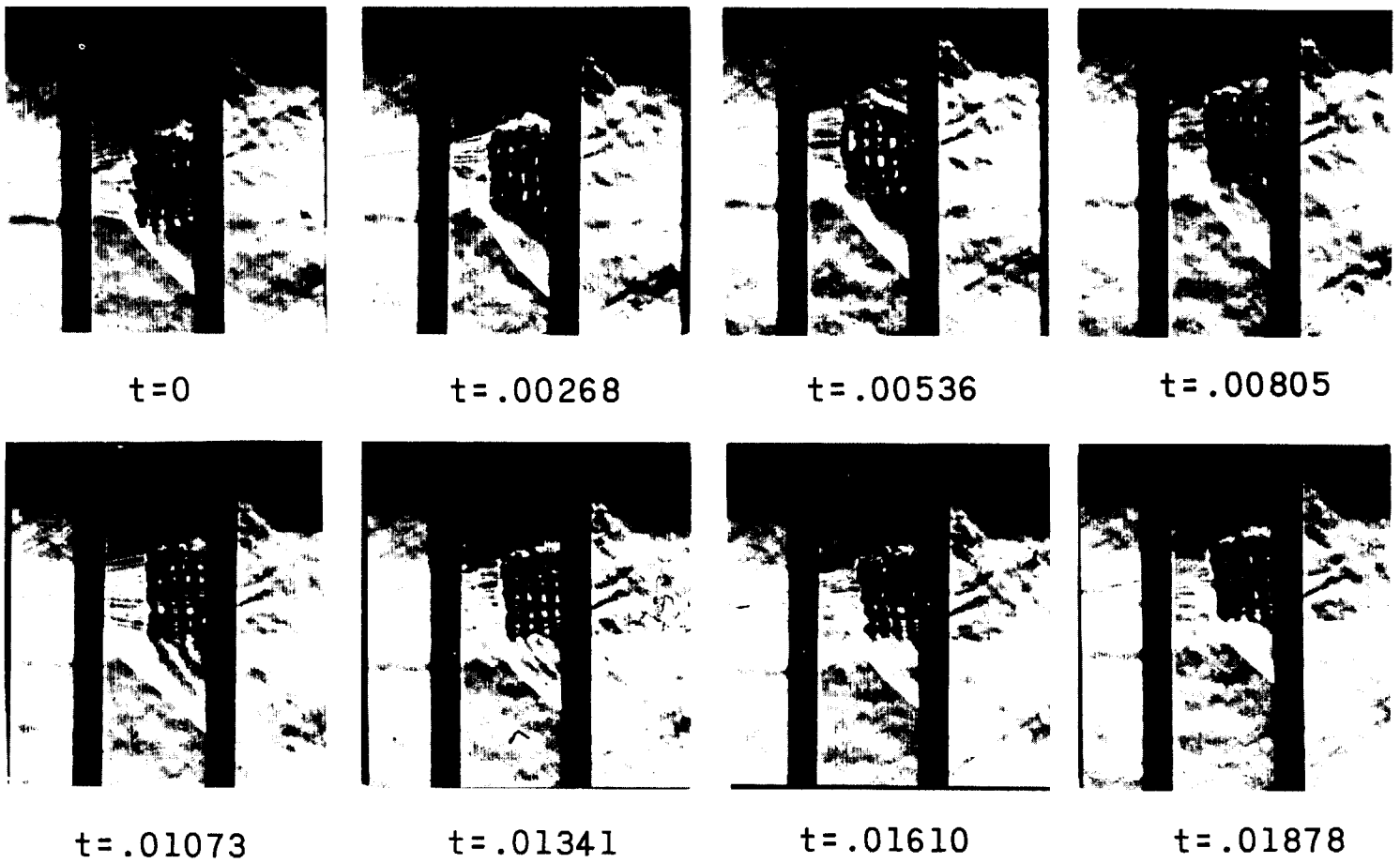

(c) Parachute 16. Mach number, 1.90; dynamic pressure, 161 lb/sq ft. L-61-44

Figure 16.- Continued.

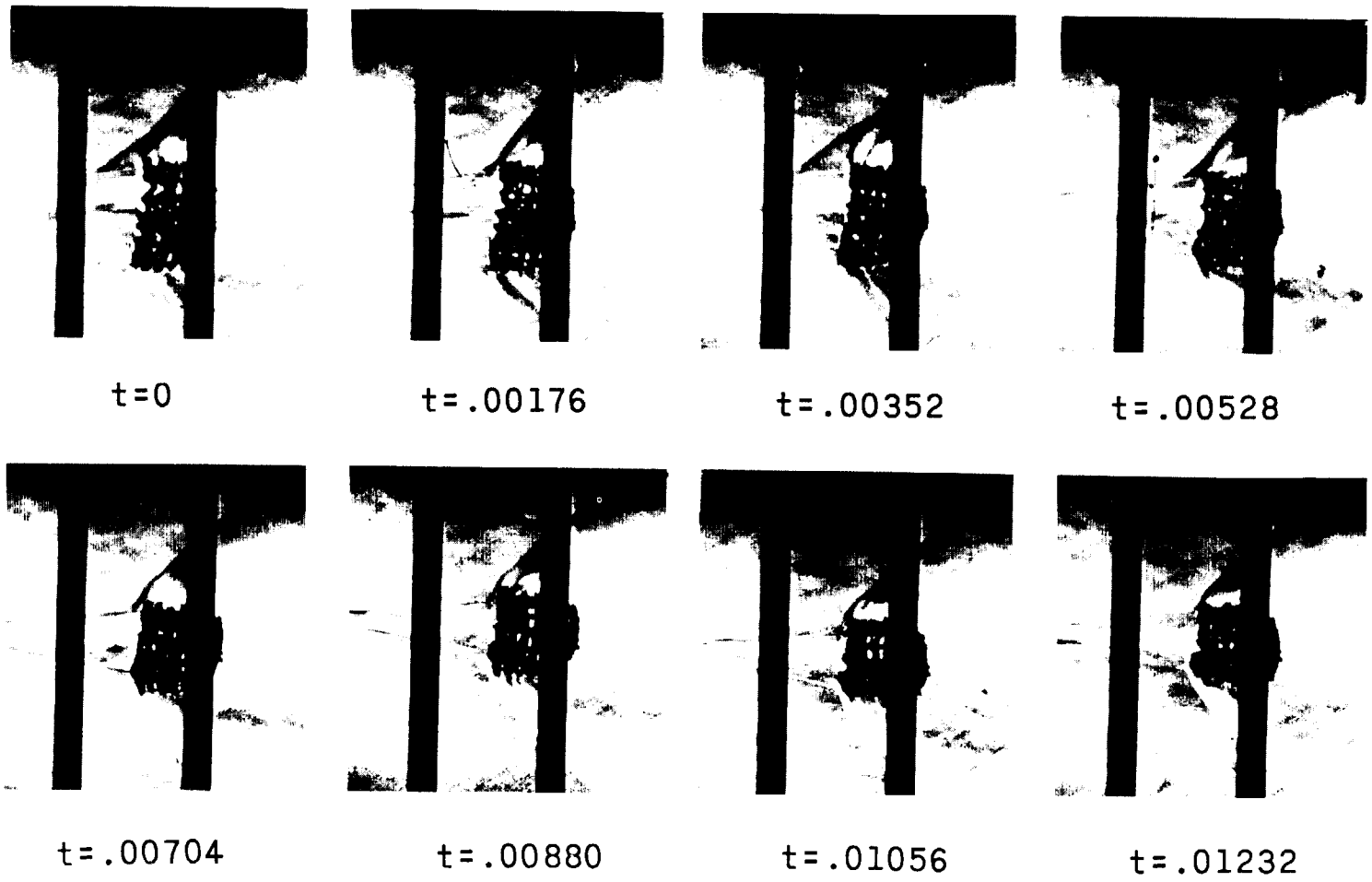

(d) Parachute 17. Mach number, 1.90; dynamic pressure, 175 lb/sq ft. L-61-45

Figure 16.- Concluded.

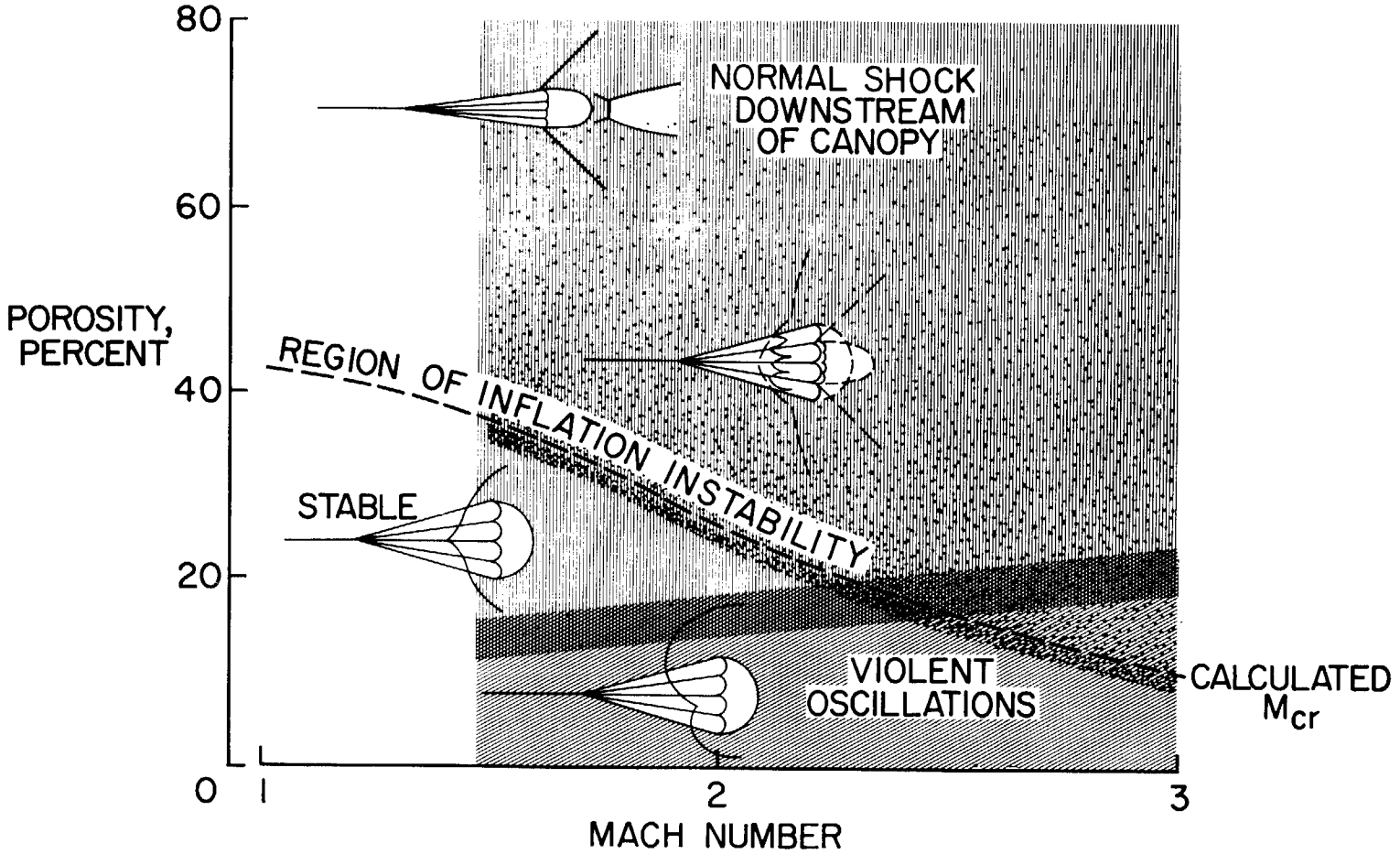

Figure 17.- Stability regions of flexible porous parachutes.

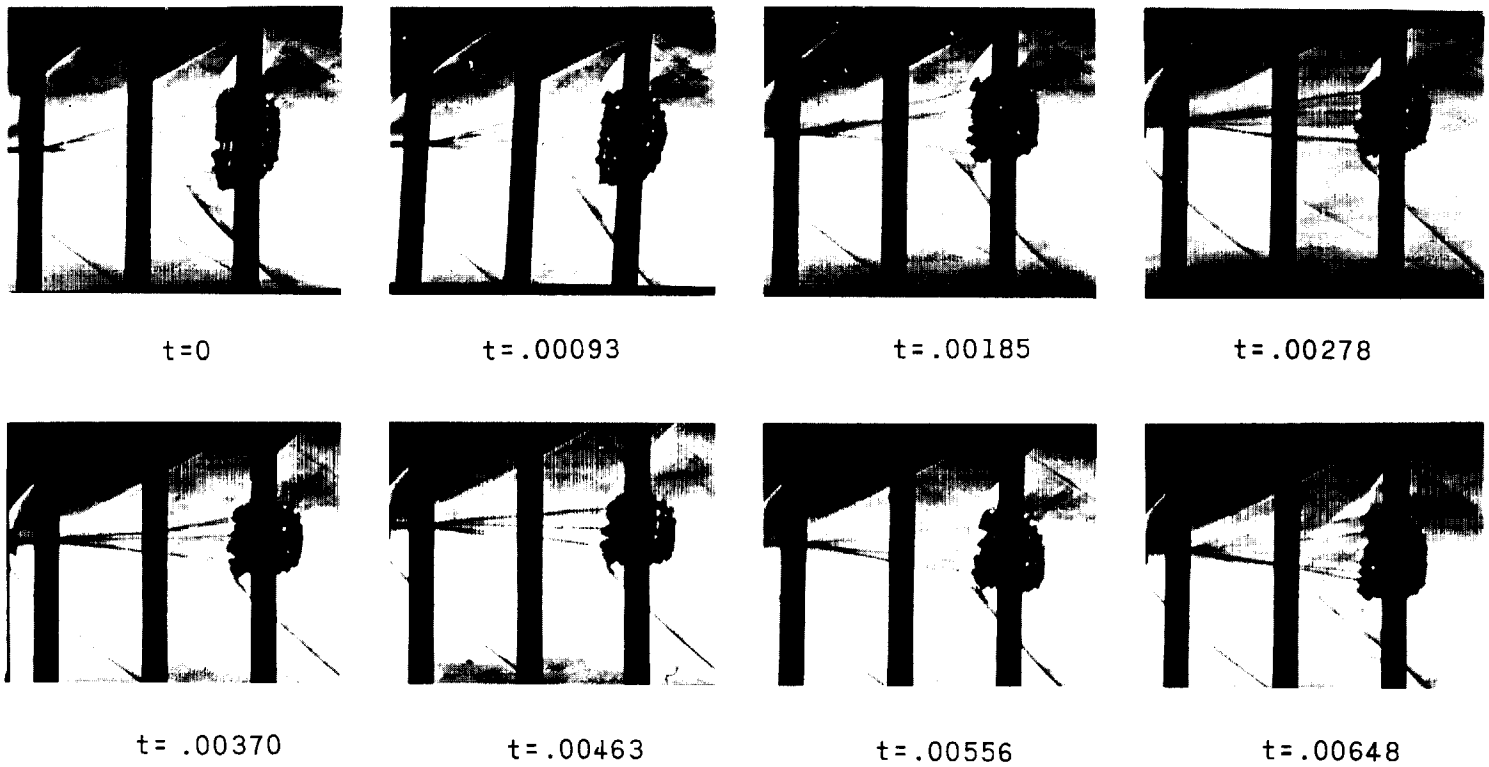

L-61-46

Figure 18.- Schlieren photographs showing change in shock pattern with time for parachute 17 with a 90° cone attached to riser line at confluence point of shroud lines. Mach number, 1.90; dynamic pressure, 175 lb/sq ft.

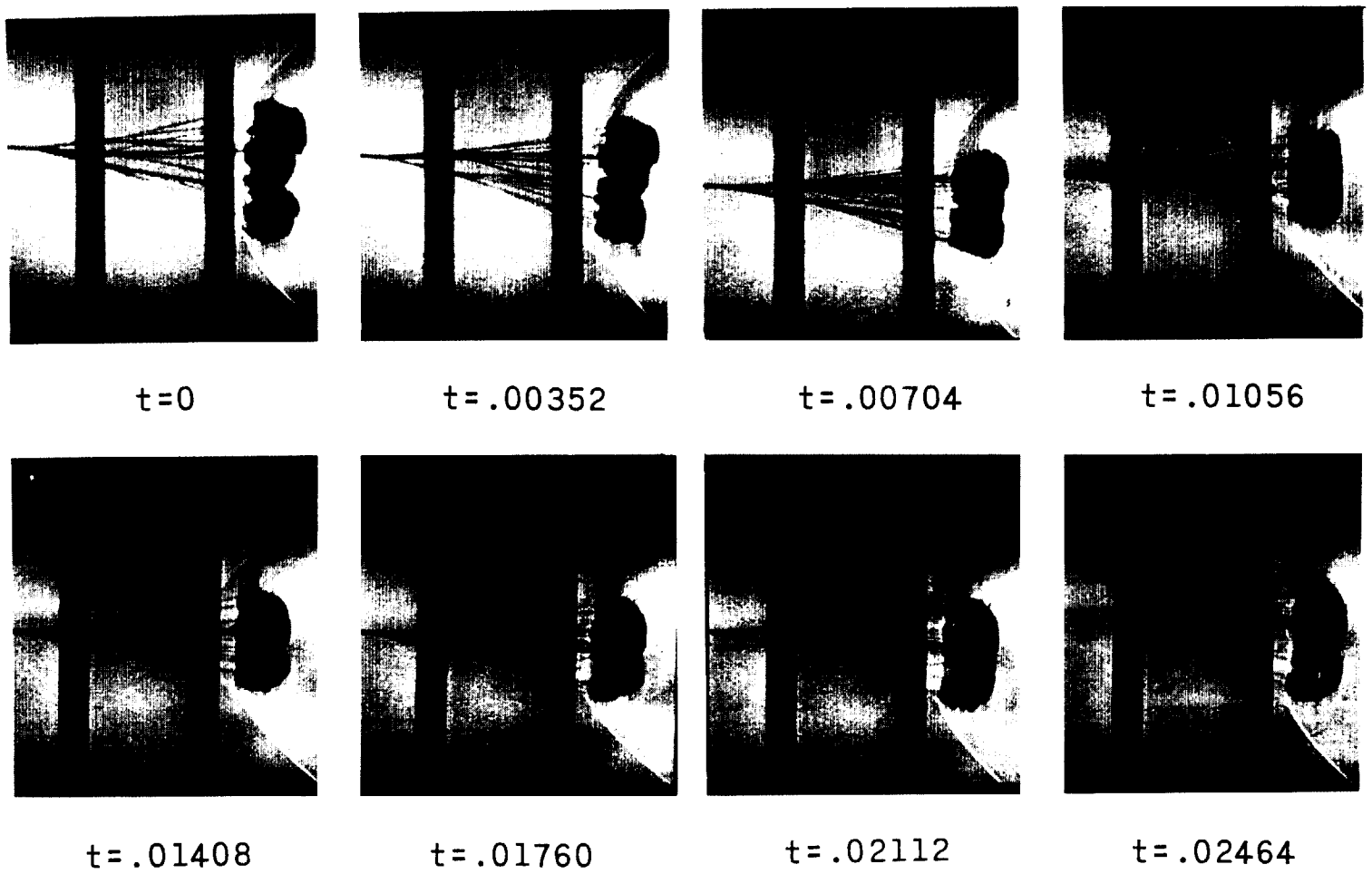

L-61-47

Figure 19.- Schlieren photographs showing change in shock pattern with time for a cluster of three flexible parachutes. Parachute 11; Mach number, 1.90; dynamic pressure, 172.03 lb/sq ft.

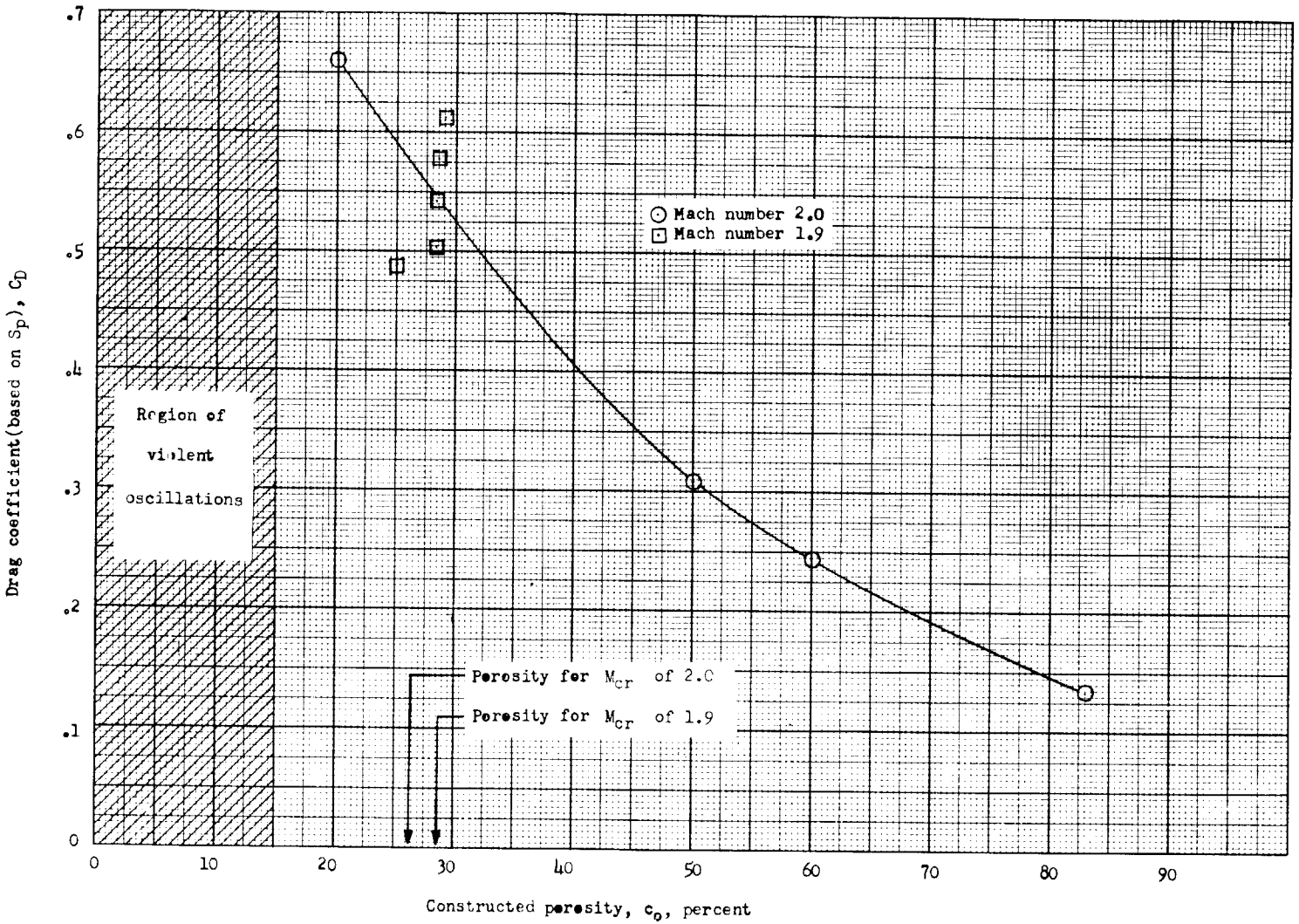

Figure 20.- Effect of porosity on drag coefficient (based on S_p) of flexible parachutes.

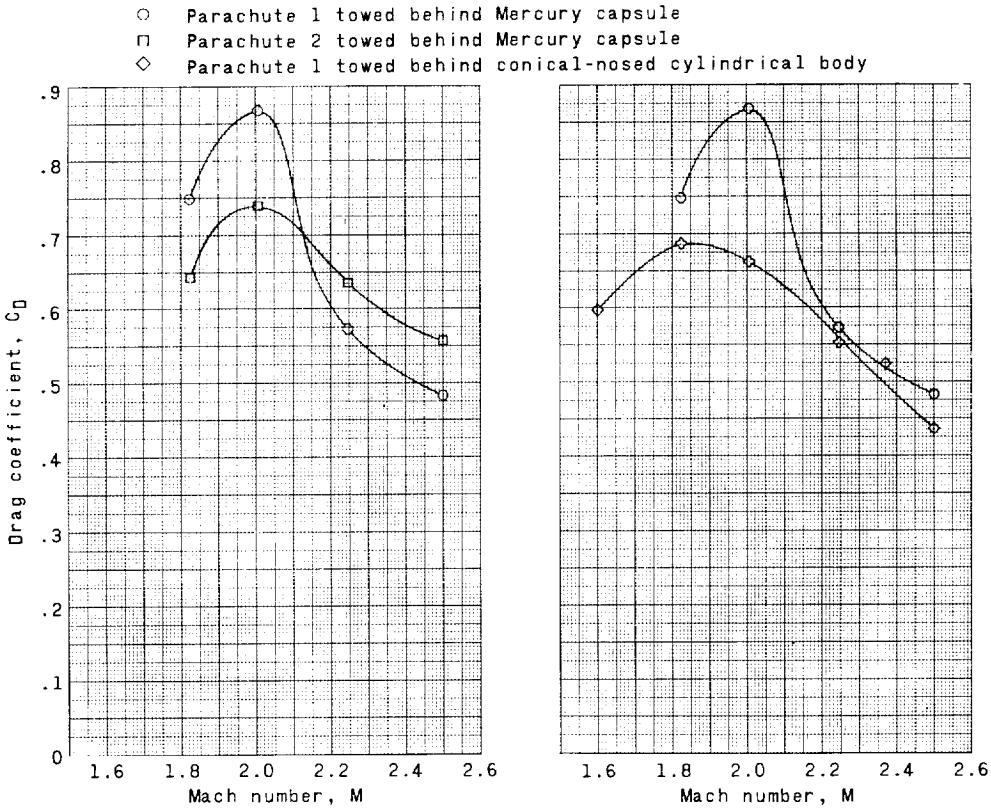

(a) Comparison of C_D for parachutes 1 and 2 towed behind Mercury capsule.

(b) Comparison of C_D for parachute 1 towed behind Mercury capsule and behind conical-nosed cylindrical body.

Figure 21.- Variation of average drag coefficient $\left(\text{based on } S_p\right)$ with Mach number for each of three configurations investigated.

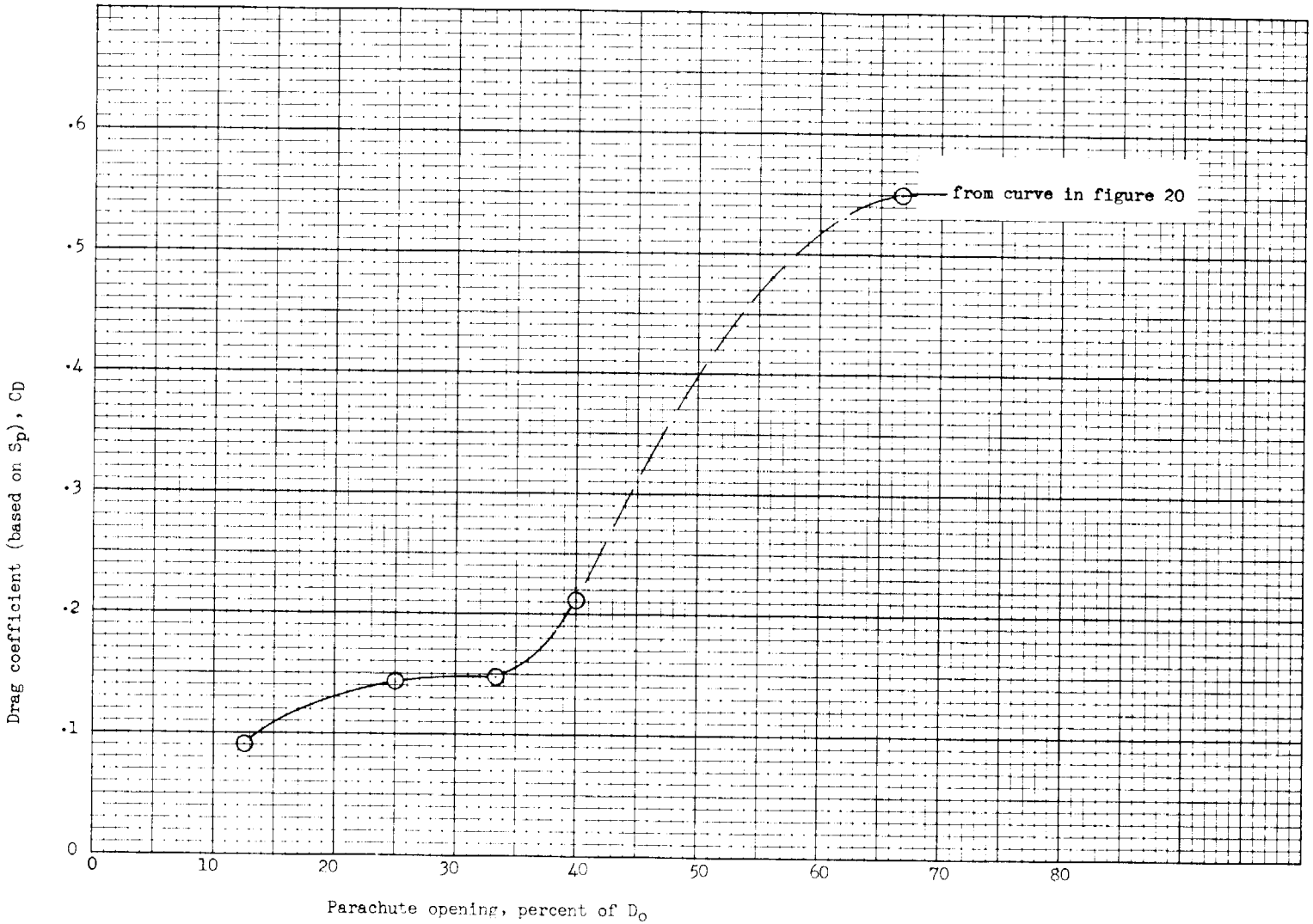

Figure 22.- Effect of parachute reefing on drag coefficient (based on S_p) at a Mach number of 2.0. Nominal diameter, D_o, 1.73 feet; constructed porosity, 28 percent.

A motion-picture film supplement is available on loan. Requests will be filled in the order received. You will be notified of the approximate date scheduled.

The film (16 mm, 28 min, B&W, silent) shows both stable and unstable regimes of flow about parachutes at supersonic speeds.

Requests for the film should be adressed to the

National Aeronautics and Space Administration
Office of Technical Information and Educational Programs
Technical Information Division (Code ETV)
Washington 25, D.C.

CUT

Date_____

Please send, on loan, copy of film supplement to NASA TN D-752 (Film serial L-598).

_____
Name of organization

_____
Street number

_____
City and State

Attention: Mr._____

Title_____

Place Stamp Here

National Aeronautics and Space Administration
Office of Technical Information and Educational Programs
Technical Information Division (Code ETV)
Washington 25, D.C.

NASA TN D-752
National Aeronautics and Space Administration.
AERODYNAMIC CHARACTERISTICS OF PARACHUTES AT MACH NUMBERS FROM 1.6 TO 3.
Julian D. Maynard. May 1961. 55p., film suppl. available on request. OTS price, $1.50.
(NASA TECHNICAL NOTE D-752)

A wind-tunnel investigation has been conducted to determine the parameters affecting the aerodynamic performance of drogue parachutes in the Mach number range from 1.6 to 3. Flow studies of both rigid- and flexible-parachute models were made by means of high-speed schlieren motion pictures, and drag coefficients of the flexible models were measured at simulated altitudes from about 50,000 to 120,000 feet.

Copies obtainable from NASA, Washington

I. Maynard, Julian D.
II. NASA TN D-752

(Initial NASA distribution: 4, Aircraft safety and noise.)

NASA

NASA TN D-752
National Aeronautics and Space Administration.
AERODYNAMIC CHARACTERISTICS OF PARACHUTES AT MACH NUMBERS FROM 1.6 TO 3.
Julian D. Maynard. May 1961. 55p., film suppl. available on request. OTS price, $1.50.
(NASA TECHNICAL NOTE D-752)

A wind-tunnel investigation has been conducted to determine the parameters affecting the aerodynamic performance of drogue parachutes in the Mach number range from 1.6 to 3. Flow studies of both rigid- and flexible-parachute models were made by means of high-speed schlieren motion pictures, and drag coefficients of the flexible models were measured at simulated altitudes from about 50,000 to 120,000 feet.

Copies obtainable from NASA, Washington

I. Maynard, Julian D.
II. NASA TN D-752

(Initial NASA distribution: 4, Aircraft safety and noise.)

NASA

NASA TN D-752
National Aeronautics and Space Administration.
AERODYNAMIC CHARACTERISTICS OF PARACHUTES AT MACH NUMBERS FROM 1.6 TO 3.
Julian D. Maynard. May 1961. 55p., film suppl. available on request. OTS price, $1.50.
(NASA TECHNICAL NOTE D-752)

A wind-tunnel investigation has been conducted to determine the parameters affecting the aerodynamic performance of drogue parachutes in the Mach number range from 1.6 to 3. Flow studies of both rigid- and flexible-parachute models were made by means of high-speed schlieren motion pictures, and drag coefficients of the flexible models were measured at simulated altitudes from about 50,000 to 120,000 feet.

Copies obtainable from NASA, Washington

I. Maynard, Julian D.
II. NASA TN D-752

(Initial NASA distribution: 4, Aircraft safety and noise.)

NASA

NASA TN D-752
National Aeronautics and Space Administration.
AERODYNAMIC CHARACTERISTICS OF PARACHUTES AT MACH NUMBERS FROM 1.6 TO 3.
Julian D. Maynard. May 1961. 55p., film suppl. available on request. OTS price, $1.50.
(NASA TECHNICAL NOTE D-752)

A wind-tunnel investigation has been conducted to determine the parameters affecting the aerodynamic performance of drogue parachutes in the Mach number range from 1.6 to 3. Flow studies of both rigid- and flexible-parachute models were made by means of high-speed schlieren motion pictures, and drag coefficients of the flexible models were measured at simulated altitudes from about 50,000 to 120,000 feet.

Copies obtainable from NASA, Washington

I. Maynard, Julian D.
II. NASA TN D-752

(Initial NASA distribution: 4, Aircraft safety and noise.)

NASA